HHS Public Access

Author manuscript

Neurobiol Dis. Author manuscript; available in PMC 2026 May 07.

Published in final edited form as:

Neurobiol Dis. 2026 February ; 219: 107267. doi:10.1016/j.nbd.2026.107267.

A *C. elegans* model of familial Alzheimer's disease shows age-dependent synaptic degeneration independent of amyloid β-peptide

Vaishnavi Nagarajan[1,†], **Caitlin L. Libowitz**[2], **Brian D. Ackley**[3], **Michael S. Wolfe**[1]

[1]Department of Medicinal Chemistry, University of Kansas, Lawrence, KS 66045, USA

[2]Graduate Program in Neurosciences, Department of Pharmacology & Toxicology, University of Kansas, Lawrence, KS 66045, USA

[3]Department of Molecular Biosciences, University of Kansas, Lawrence, KS 66045, USA

Abstract

The membrane-embedded γ-secretase complex is involved in the intramembrane cleavage of ~ 150 substrates. Cleavage of amyloid precursor protein (APP)-derived substrate C99 generates 38–43-residue secreted amyloid β-peptides (Aβ), with the aggregation-prone 42-residue form (Aβ42) particularly implicated in the pathogenesis of Alzheimer's Disease (AD). However, whether Aβ42 is the primary driver of neurodegeneration in AD remains unclear. Dominant mutations in APP or presenilin—the catalytic component of γ-secretase—cause early-onset familial AD (FAD) and reduce one or more steps in the multi-step processive proteolysis of C99 to Aβ peptides, apparently through stabilization of γ-secretase enzyme-substrate (E-S) complexes. To investigate mechanisms of neurodegeneration in FAD, we developed new *C. elegans* models co-expressing wild-type or FAD-mutant C99 substrate and presenilin-1 (PSEN1) variants in neurons, allowing intramembrane processing of C99 to Aβ *in vivo.* We demonstrate that while FAD-mutation of either C99 or PSEN1 leads to age-dependent synaptic loss, proteolytically inactive PSEN1 did not. Designed mutations that allow stable E-S complex formation without Aβ42 or Aβ production likewise result in synaptic degeneration. Moreover, replacement of C99 with variants of a Notch1-based substrate revealed that disrupted processing of another γ-secretase substrate can similarly lead to synaptic degeneration. These results support a model in which synaptic loss can be triggered by toxic, stalled γ-secretase E-S complexes in the absence of Aβ production and not by simple loss of proteolytic function. This new *C. elegans* system provides a powerful platform to study the role of dysfunctional γ-secretase substrate processing in FAD pathogenesis.

Keywords

Amyloid precursor protein; presenilin; γ-secretase; enzyme-substrate complex; gain of function

Corresponding author: mswolfe@ku.edu (co-corresponding author: bdackley@ku.edu).

[†]Present address: School of Natural Sciences (Biology), Northwest Missouri State University, Maryville, MO

Author Contributions: V.N.: methodology, data curation, formal analysis, writing—original draft, visualization; C.L.L.: methodology, data curation, formal analysis, writing—original draft, visualization; B.D.A: conceptualization, writing—reviewing and editing, supervision, project administration, resources; M.S.W.: conceptualization; writing—reviewing and editing, supervision, project administration, funding acquisition.

INTRODUCTION

Alzheimer's disease is a progressive neurodegenerative disorder causing cognitive decline and dementia in over 50 million people worldwide (Breijyeh and Karaman 2020). AD is pathologically characterized by cerebral deposition of two proteins: amyloid β-peptide (Aβ), forming extra-neuronal plaques, and the microtubule-associated protein tau, forming intraneuronal fibrillary tangles (Cai and Tammineni 2017). Synaptic damage and degeneration occur in early stages, eventually leading to neuronal loss (Pelucchi, Gardoni et al. 2022). Alterations in axonal transport of synaptic vesicles, mitochondrial damage, neuroinflammation, and oxidative stress leading to axonal dystrophy have been implicated in synaptic loss in AD (Krstic and Knuesel 2013, Subramanian, Savage et al. 2020).

Aβ aggregation has long been considered the initiator of synaptic damage and neurodegeneration, per the amyloid hypothesis of AD pathogenesis. Aβ is produced from APP by sequential proteolysis by β-secretase, which sheds the large lumenal/extracellular ectodomain, and γ-secretase, which cleaves the remnant 99-residue fragment (C99) within its single transmembrane domain (Zhang, Ma et al. 2012). Rare dominant missense mutations in APP and presenilin, the catalytic component of γ-secretase, cause early-onset familial AD (FAD)(Goate, Chartier-Harlin et al. 1991, Sherrington, Rogaev et al. 1995), with the same pathology, presentation and progression as the more common sporadic late-onset AD (Bateman, Aisen et al. 2011, Morris, Weiner et al. 2022), strongly suggesting common pathogenic mechanisms. These mutations alter Aβ production and properties, generally increasing the proportion of the aggregation-prone 42-residue peptide (Aβ42) over the more soluble 40-residue variant (Aβ40) (Tanzi 2012). Nevertheless, after over 30 years of the amyloid hypothesis, mechanisms by which Aβ aggregates trigger synaptic and neuronal degeneration remain unresolved (Makin 2018). Moreover, therapeutic candidates targeting Aβ repeatedly failed in clinical trials until the recent approval of monoclonal antibodies. These new antibodies, however, are controversial, due to concerns about efficacy and safety (Hunter 2024).

The lack of mechanistic understanding and limited effectiveness of therapeutics suggests that Aβ may not be the primary disease driver in AD. FAD mutations, however, are only found in genes encoding the substrate (APP) or enzyme (γ-secretase) that produce Aβ, pointing to alteration of proteolytic processing by γ-secretase in pathogenesis. Proteolysis of C99 by γ-secretase is complex: initial endoproteolysis produces long Aβ peptide intermediates Aβ48 or Aβ49 that are then processively trimmed, generally in tripeptide increments, to shorter secreted forms (Takami, Nagashima et al. 2009). We found that FAD mutations in APP and PSEN1 are consistently deficient in early processing steps, rather than later steps that produce Aβ40 and Aβ42 (Devkota, Williams et al. 2021, Devkota, Zhou et al. 2024, Arafi, Devkota et al. 2025, Devkota, Maesako et al. 2025). Moreover, we found that FAD mutations stabilize the enzyme-substrate complex, suggesting a mechanism for the reduced proteolytic function (Levitan, Doyle et al. 1996, Devkota, Zhou et al. 2024, Arafi, Devkota et al. 2025, Devkota, Maesako et al. 2025).

To test mechanisms by which FAD mutations trigger neurodegeneration, we developed a *C. elegans* transgenic model system that expresses C99 and/or PSEN1 in neurons (Devkota,

Zhou et al. 2024). C99 includes a signal sequence for membrane insertion, and PSEN1 replaces *C. elegans* orthologs *sel-12* and *hop-1* to provide functional γ-secretase with the human catalytic component (Levitan, Doyle et al. 1996). Thus, in this system Aβ is produced from substrate and enzyme via intramembrane proteolysis, as it is normally, in contrast to previous *C. elegans* models that expressed Aβ directly and in the cytosol. Using this system, we found that FAD mutations lead to age-dependent synaptic degeneration and reduced lifespan. Moreover, this phenotype did not require Aβ production and implicated the stalled enzyme-substrate complex as the pathogenic trigger. Here we reproduce these findings in independent transgenic lines and extend these studies by showing that the neurodegenerative phenotype is not due to simple loss of proteolytic function of stalled complexes. We also test the ability of another γ-secretase substrate, Notch1, to induce the neurodegenerative phenotype and find that a cleavage-deficient mutant Notch1 substrate likewise results in age-dependent synaptic loss. Taken together, these results suggest that stalled γ-secretase enzyme-substrate complexes *per se* trigger a novel gain of synaptotoxic function.

RESULTS

Previous attempts to develop a *C. elegans* model for Alzheimer's disease involved expression of the amyloid β-peptide (Aβ), particularly Aβ42, which pathologically deposits in the Alzheimer brain (Link 1995, Bieschke, Cohen et al. 2009, McColl, Roberts et al. 2009, Treusch, Hamamichi et al. 2011, McColl, Roberts et al. 2012). However, Aβ is normally produced in cellular membranes through sequential proteolysis of the amyloid precursor protein (APP), first by β-secretase to produce the membrane-bound C-terminal APP stub C99, followed by intramembrane cleavage by γ-secretase. Dominant FAD-causing missense mutations in the substrate or enzyme alter the proteolytic processing of APP by γ-secretase. An *in vivo* model that recapitulates the proteolytic processing of APP substrate, as it occurs naturally, is critical to understanding how FAD mutations contribute to pathogenesis. Such *C. elegans* models, in which Aβ production occurs through γ-secretase in membranes had not been previously described. For these reasons, we engineered novel *C. elegans* models that co-express membrane-associated human C99 and human PSEN1 in neurons to allow for intramembrane proteolysis to produce Aβ.

We designed transgenes that express human wt C99APP or human wt PSEN1 with the *rgef-1* promoter, which drives stable transgene expression with age pan-neuronally in *C. elegans* (Chen, Fu et al. 2011) (Adamla and Ignatova 2015) (Munoz-Jimenez, Ayuso et al. 2017). The APP N-terminal signal peptide sequence precedes the C99APP sequence to allow membrane insertion. *unc-54* 3' UTR was used to promote transgenic expression in somatic cells (Merritt, Rasoloson et al. 2008). Additionally, C99APP and PSEN1 variant transgenes were created using the same expression vector (Figure 1a). Transgenic worms were obtained by microinjection of human C99APP and human PSEN1 constructs in the *juIs1* line (Hallam and Jin 1998), which expresses GFP-fused synaptobrevin protein in presynaptic terminals of GABAergic motor neurons, visualized as synaptic puncta along the dorsal and ventral nerve cords. Schematic representation of γ-secretase tripeptide cleavage driven by three active site pockets (S1', S2' and S3') of presenilin (PSEN) is shown along with the corresponding three amino acids (P1', P2' and P3') of substrate in

Figure 1b. We previously showed that co-expression of mutant C99APP and PSEN1 led to neurodegeneration phenotypes (Devkota, Zhou et al. 2024).

C. elegans lines co-expressing wt C99APP and wt PSEN1 showed lifespans that were comparable to those of the parental line *juIs1* (Figure S1a). The log rank test of the survival curves showed that there is no statistically significant difference (P = 0.851). Numbers of synaptic puncta in transgenic lines were similar to those of the parental line for each day examined (Days 1–7 & 9) (Figure S1b).

wt PS-1 exacerbates I45F C99-induced synaptic loss in *C. elegans*.

The Iberian mutation in APP, I45F (Aβ/C99 numbering; I716F in the 770-residue isoform of APP), is an FAD mutation that places Phe in the P2' position relative to Aβ46→Aβ43 tripeptide trimming. We have previously demonstrated that Phe in the P2' position with respect to any cleavage event in the processive proteolysis of C99 substrate by γ-secretase blocks that cleavage step. Thus, for I45F the production of Aβ43 is prevented while allowing Aβ45→Aβ42 cleavage, thereby increasing the Aβ42/Aβ40 ratio (Bolduc, Montagna et al. 2016) (Figure 2a). The median lifespan of both I45F C99APP-expressing lines (with and without coexpression of wt PSEN1) were shorter than wt C99APP + wt PSEN1 animals, although wt PSEN1 coexpression resulted in substantial reduction in lifespan and early loss of synapses (Figure 2b; Table S1). *C. elegans* lines that express I45F C99APP and wt PSEN1 showed loss of synaptic puncta beginning on day 3 in dorsal and ventral nerve cords, with substantial synaptic degeneration occurring by day 9 in the dorsal cord. In contrast, the monogenic line expressing I45F C99APP alone showed only slight loss of synaptic puncta in the dorsal cord on day 9. (Figure 2c–d). We observed similar results in additional independent lines with the same transgenes, as reported in our previous study (Devkota, Zhou et al. 2024). These results indicate that I45F C99APP induces a weak neurodegenerative phenotype—likely due to interaction with endogenous presenilin SEL-12 and/or HOP-1—that is strongly exacerbated by coexpression of wt human PS-1, demonstrating a genetic interaction between the two transgenes.

Synaptic loss is triggered independently of Aβ42.

Addition of a designed V44F mutation to the Iberian FAD-mutant C99APP (V44F/I45F C99APP) eliminates the production of Aβ42 by blocking processive proteolysis by γ-secretase at the Aβ45→Aβ42 step, as Phe is located in the P2' position relative to this cleavage site, along with blocking Aβ46→Aβ43 due to I45F (Figure 3a) (Pope, Wilkins et al. 2021, Devkota, Zhou et al. 2024). Thus, this double mutant can address whether Aβ42 is required for the synaptic degeneration observed with I45F mutation alone. The median lifespan of V44F/I45F C99 APP + wt PSEN1 was substantially shorter than wt C99APP + wt PSEN1, while expression of V44F/I45F alone attenuated this effect (Figure 3b). The survival curves of wt C99APP + wt PS-1 and V44F/I45F C99 APP + wt PSEN1 were significantly different based on Holm-Sidak pairwise comparison (Table S2) (Cardillo 2006). Similarly, significant loss of synaptic puncta was seen in dorsal and ventral nerve cords on day 2 in lines neuronally co-expressing V44F/I45F C99APP and wt PSEN1. A less severe phenotype with a delayed onset and absence of further synaptic loss was seen in the monogenic V44FI45F C99APP line (i.e., age-dependent loss of synaptic puncta was not

observed in this control) (Figure 3c–d), recapitulating observations of an independent line with same mutations (Devkota, Zhou et al. 2024). These observations collectively suggest that Aβ42 is not essential for the neurodegenerative phenotype of these lines.

Synaptic loss is triggered independently of Aβ.

V50F/M51F mutation in C99APP blocks the initial endoproteolytic (ε) cleavage that releases APP intracellular domain and generates intermediates Aβ_{48} and Aβ_{49}, due to the presence of Phe in the P2' pocket relative to either cleavage site. This prevents C99APP substrate from being processed to Aβ, thereby providing a substrate suitable for testing if synaptic degeneration is dependent on any form of Aβ (Figure 4a). While V50F/M51F C99APP is not proteolyzed by γ-secretase, binding of this substrate to the protease is not affected (Bolduc, Montagna et al. 2016). Lifespan of animals expressing V50F/M51F C99APP + wt PSEN1 was reduced similarly to that of those coexpressing wt PSEN1 pIus either I45F C99APP or V44F/I45F C99APP, as measured by median survival times (Figure 4b). Pairwise comparison of the survival curves showed that there is a significant difference between wt C99APP + wt PSEN1 and V50F/M51F C99APP + wt PSEN1 (Table S3) . A reduced number of synaptic puncta was seen in the dorsal cord of these lines from as early as day 1 of adulthood compared to wt + wt transgenic lines (Figure 4c–d). In contrast, co-expression of wt PSEN1 with V50F/M51F C99APP led to fewer synaptic puncta in the ventral compared to wt control animals on day 3. However, an increase in synaptic puncta was observed in V50F/M51F C99APP mutants from day 7 in both nerve cords, a phenomenon not seen in lines co-expressing I45F or V44F/I45F C99APP with wt PS-1. The increase in synaptic puncta following decline cannot be explained by survivor bias, as the upper limit on earlier days is below the upper limit on later days (i.e., worms fated for longer survival should be among the earlier cohorts). This aligns with our observation of independent lines described in our previous study and confirms that prevention of Aβ formation does not rescue loss of synaptic puncta, while supporting mechanisms of regeneration in this model (Devkota, Zhou et al. 2024).

L166P PSEN1-induced synaptic loss is dependent on C99APP coexpression.

The median lifespan in our new *C. elegans* lines expressing PSEN1 L166P FAD mutation, irrespective of the presence of C99APP substrate, was reduced compared to that of wt C99APP + wt PSEN1 animals (Figure 5a; Table S4). wt C99APP + L166P lines also displayed age-dependent decline in the numbers of synaptic puncta in both cords (Figure 5b,c), results consistent with independent lines studied earlier (Devkota, Zhou et al. 2024). In our previous study, however, imaging of synaptic puncta in monogenic PSEN1 L166P lines was not possible due to toxic sensitivity to the anesthetic. This problem was solved here by immobilizing animals with polystyrene beads, which revealed that monogenic PSEN1 L166P *C. elegans* did not show significant age-dependent synaptic degeneration, with results indistinguishable from wt C99APP + wt PSEN1 lines for both the dorsal and ventral cords (Figure 6a,b). There was some slight change in the average number of synapses within the PSEN1 L166P strain itself over time, but only in the dorsal cord, and not in comparison to controls. These observations indicate that co-expression of exogenous substrate is necessary for synaptic degeneration in this experimental system, while the shortened lifespan is independent of substrate co-expression. This is the sole instance where

shortened lifespan and age-dependent synaptic loss did not correlate, suggesting that, at least in the monogenic L166P PSEN1 lines, the two phenotypes are caused by distinct mechanisms.

Synaptotoxic effects are not specific to dysfunctional proteolysis of C99APP substrate

To determine if stalled E-S complex formed between mutant PSEN1 with a substrate other than C99 can affect proteolysis by γ-secretase, we created human Notch1-based transgenic DNA encoding a C-terminal fragment analogous to C99APP (C99Notch1) as well as its V50F/L51F double mutation, designed to block ε cleavage when either Phe is positioned at P2' during proteolytic processing by the enzyme. We have recently reported using mass-spectrometry and ELISA that V50F/L51F double mutation results in ~50% reduction in proteolysis of Notch-1 substrate by γ-secretase (Malvankar and Wolfe 2025), similar to but not as substantial as the near complete block of proteolysis of the analogous V50F/M51F in C99APP (Bolduc, Montagna et al. 2016). To test the effects of this double mutation on synaptic degeneration in *C. elegans*, expression vectors were designed to comprise of codons for signal peptide (as used in C99APP constructs) followed by 99 amino acids of the Notch1 extracellular truncation (NEXT) C-terminal fragment, generated from ligand-dependent juxtamembrane cleavage by ADAM-10 and a direct substrate for γ-secretase (Brou, Logeat et al. 2000, Mumm, Schroeter et al. 2000). wt C99Notch1 and mutant C99Notch1 transgenes were designed with *rgef-1* pan-neuronal promoter and *unc-54* 3' UTR as used in C99APP expression vectors (see Supporting Information for full DNA sequences). Note that this truncated form of Notch1 does not contain regions responsible for nuclear localization and transcriptional regulation.

Co-expression of V50F/L51F C99Notch-1 with wt PSEN1 resulted in shorter median lifespan in both independent lines compared to *juIs1* and wt Notch-1 + wt PSEN1, based on a cut-off standard for statistical signifance of $p > 0.05$ (Figure 7a & Figure S2a). The survival curves of V50F/M51F C99Notch-1 + wt PS-1 mutants versus wt C99Notch-1 + wt PS-1 were statistically different based on pairwise comparisons using the Holm-Sidak method (Table S5). Synaptic loss occurred as early as day 1 in V50F/M51F C99Notch-1 animals co-expressing wt PSEN1 in both nerve cords (Figure 7b–7c & Figure S2b–S2c). These results suggest that stalled γ-secretase complexes can be formed from dysfunctional proteolysis of a substrate other than C99APP and trigger synaptotoxicity in *C. elegans*. However, because cleavage of V50F/M51F double mutation in C99Notch-1 is only partially reduced, the possibility remains that inefficiently trimmed Nβ proteolytic products (Notch counterparts to Aβ) contribute to the observed phenotype.

Catalytic inactive PSEN1 does not lead to reduced lifespan or synaptic degeneration.

To test whether synaptic degeneration and reduction in lifespan is due to a simple loss of proteolytic function of γ-secretase, we utilized a PSEN1 transgene containing a mutation in one of the catalytic aspartates (D257A). Three independently derived lines containing the human D257A PS1 construct were obtained after microinjection and assessed for both synapse degeneration and lifespan. When assessed for median survival, none of the PSEN1 D257A mutant lines showed significantly reduced lifespan compared to parental strain *juIs1* (Figure 8a; Table S7). wt PS-1 + wt C99APP animals from strain *lhEx661* had longer

median lifespans compared to parental line *juIs1* and two lines transgenic for D257A PS1 but were not statistically significant. The third D257A PS1 line had a significantly longer lifespan compared to *juIs1,* but not to the other two transgenic lines containing D257A PS1. This is likely due to variability in transgene expression between the three independently derived lines.

Interestingly, animals expressing D257A PSEN1 transgene had a slight visible egg-laying deficient phenotype, with abnormal protruding vulva. Egg-laying deficiency is present in animals with loss-of-function mutations in *sel-12*, a homolog of human Presenilin in *C. elegans*, and is linked to deficiencies in cleavage of *lin-12* family of receptors (NOTCH receptors in *C. elegans*) (Levitan and Greenwald 1995). These visible protruding vulva defects prompted us to determine whether other aspects of nematode health known to be affected by *sel-12* deficiency, specifically brood size and embryonic viability, were affected. Animals expressing D257A PSEN1 showed significant differences in brood size, and one line showed significant defects in embryonic viability (Figure 8b; see also Figure S3 for brood size and embryonic viability for all other transgenic lines in this study). While the other two D257A PSEN1 lines did not show significant changes in embryonic viability, they were slightly decreased compared to both *juIs1* and WT PSEN1 + WT APP C99 animals. In all lines, there were no overall significant differences between synapse numbers compared with parental line *juIs1* or wt C99APP + wt PSEN1 in either cord on any given day, indicating no age-dependent synapse degeneration (Figure 8c). Together, these results indicate that a simple loss of function of enzymatic activity is not sufficient to lead to synaptic degeneration and a reduced lifespan. The *sel-12*-like loss-of-function phenotypes (effects on brood size and embryonic viability) indicate that distinct pathways are involved.

DISCUSSION

The amyloid cascade hypothesis of AD pathogenesis, first formulated over 30 years ago, implicates aggregated Aβ, particularly Aβ42, in triggering downstream neurotoxicity and synaptic dysfunction, ultimately leading to cognitive dysfunction. This hypothesis emerged with the discovery of FAD-associated dominant missense mutations in the APP gene, in and around the small Aβ region of the much larger precursor protein. The subsequent discovery of presenilin genes as sites of FAD mutations, that these mutations elevate the Aβ42/Aβ40 ratio, and that presenilins are proteases, the catalytic component of γ-secretase, seemingly cemented the amyloid hypothesis. All FAD mutations are found in the substrate and enzyme that produce Aβ, and these mutations alter the production or properties of Aβ peptides.

Decades later, fundamental gaps remain regarding the nature of pathogenic Aβ assemblies, the identity of cognate receptors, and pathways that relay synaptotoxic signals. In addition, monoclonal antibodies against Aβ aimed at halting the amyloid cascade and preventing neurodegeneration have shown only modest slowing of cognitive decline, despite effective clearance of amyloid plaques (Kurkinen, Fulek et al. 2023). For these reasons, we reinvestigated the identity of the pathogenic initiator in FAD. Through biochemical, structural, computational and cellular studies, we recently found that FAD mutations are deficient in multiple proteolytic steps in the processing of APP C99 substrate by γ-secretase due to stalling/stabilization of the enzyme-substrate (E-S) complex (Devkota, Zhou et al.

2024). Establishment of a *C. elegans* model system for FAD then provided a means of testing mechanisms of synaptotoxicity, leading to the conclusion that stalled γ-secretase E-S complexes, even in the absence of Aβ or in the presence of a substrate other than C99APP, can trigger synaptic loss.

In the present study, we provide important confirmation and extension of the "stalled complex" hypothesis of FAD pathogenesis (Wolfe 2025). Through the generation of independent transgenic *C. elegans* lines, we demonstrate that the FAD APP Iberian mutation I45F (Aβ numbering; I716F APP770 numbering) elicits age-dependent synaptic loss and reduced lifespan that is largely dependent on co-expression of human wt PS1. This mutation leads to substantial elevation of the Aβ42/Aβ40 ratio, primarily by blocking γ-secretase trimming of Aβ46 to Aβ43, thereby reducing Aβ40 production (Bolduc, Montagna et al. 2016). However, addition of the designed V44F mutation, which further blocks trimming of Aβ45 to Aβ42, does not rescue the neurodegenerative phenotype. Moreover, installation of the designed V50F/M51F double mutation near the initial γ-secretase cleavage site in APP C99—blocking all Aβ production even though this mutant substrate can nevertheless bind the protease complex—likewise leads to the neurodegenerative phenotype. These findings show that the age-dependent synaptic loss is not dependent on Aβ42 or overall Aβ production and are consistent with stalled E-S complexes as the pathogenic trigger.

We further observed that neuronal expression of FAD-mutant PSEN1 L166P leads to reduced lifespan in *C. elegans*, even in the absence of APP C99 coexpression, consistent with our previous report (Devkota, Zhou et al. 2024). In the present study, however, we observed the first disconnect in our new transgenic *C. elegans* FAD model system between reduced lifespan and age-dependent synaptic loss: Animals transgenic for PSEN1 L166P without wt C99APP showed reduced lifespan without significant synaptic degeneration. This new observation suggests that in this model system there may be multiple pathways and mechanisms by which PSEN1 FAD mutations might affect lifespan, many of which may not be coupled to synaptic degeneration. This finding further suggests that synaptic degeneration due to L166P PSEN1 in this model system requires co-expression of exogenous substrate to increase levels of stalled E-S complexes. Note that in a mouse model with PSEN1 and PSEN2 conditionally knockout in excitatory neurons of postnatal forebrain and with only a single allele with knock-in of L435F PSEN1 FAD mutation, cortical neurodegeneration was observed in the presence or absence of endogenous APP expression (Yan, Zhang et al. 2024). However, the L435F mutation is severely deficient in proteolytic function, making this genetic mouse model nearly as functionally deficient as a complete PSEN1/PSEN2 conditional knockout, a situation that does not occur in any cases of FAD (see below).

We hypothesized that, with FAD-mutant PSEN1, formation of stalled γ-secretase E-S complexes with other substrates could trigger synaptic degeneration. Consistent with this idea, we observed in two independent transgenic lines that neuronal co-expression of WT PSEN1 and V50F/L51F Notch1-based substrate, which is cleaved 50% less efficiently by γ-secretase than its wt counterpart (Malvankar and Wolfe 2025), led to synaptic loss and a shorter median lifespan in our *in vivo* model. This shows that synaptic loss in *C. elegans* can be triggered by stalled E-S complexes with a substrate other than APP C99. This finding is consistent with the recent study, mentioned above, demonstrating that a PSEN1

FAD mutation can cause neurodegeneration in the absence of APP in mice (Yan, Zhang et al. 2024). γ-Secretase has broad substrate specificity, with ~150 known membrane protein substrates (Güner and Lichtenthaler 2020). We suggest that FAD-mutant PSEN1/γ-secretase can form stalled E-S complexes with all or most of these other substrates to elevate total levels of synaptotoxic stalled E-S complexes.

We further show in this study that a simple loss of γ-secretase catalytic activity is not sufficient to cause the observed synaptic loss and reduced lifespan seen with FAD mutants. Three transgenic *C. elegans* lines were generated that neuronally express PSEN1 D257A, which contains a mutation of one of the essential conserved aspartate residues in the active site, thereby rendering this mutant PSEN1 catalytically inactive. This finding is consistent with two observations about human FAD. First, although over 300 FAD-associated mutations in PSEN1 have been identified, including many in and around the active site, neither of the two catalytic aspartates are mutated in any case of FAD. Indeed, no FAD mutation has been found that leads to complete loss of proteolytic activity. Second, dominant loss-of-function mutations in PSEN1 and other components of the γ-secretase complex, resulting in nonsense-mediated decay of the mRNA and haploinsufficiency, are associated with hereditary acne inversa, not neurodegeneration (Wang, Yang et al. 2010). Thus, although FAD mutations result in reduced proteolytic function, this partial loss of function alone apparently cannot elicit FAD. Presenilin proteolytic function does appear to be disrupted in the animals expressing PSEN1 D257A, as indicated by the observed *sel-12*-like egg-laying defect. Thus, loss of proteolytic function alone does not lead to age-dependent synaptic degeneration or reduce lifespan in this *C. elegans* model system. Whether co-expression of wt C99APP with PSEN1 D257A causes synaptic degeneration and reduces lifespan in these animals remains to be determined, and synergistic effects between reduction of proteolytic function and gain of new synaptotoxic function, both due to stalled γ-secretase E-S complexes, are still possible.

Our findings clearly point to stalled E-S complexes *per se* as an initiator of synaptic loss in this transgenic model organism. In humans with AD, synaptic density correlates with cognitive function (DeKosky and Scheff 1990). The transgenic *C. elegans* system described here may provide a valuable model to understand mechanisms of synaptic dysfunction observed in all AD, not only FAD. In sporadic late-onset AD, with no mutation in APP or presenilin, other factors may lead to stalled γ-secretase E-S complexes; for instance changes in membrane composition or intracellular or intraorganelle pH. γ-Secretase is a membrane-embedded aspartyl protease that cleaves within the transmembrane domain of its many substrates. Altered cholesterol levels can affect γ-secretase activity in cells and proteoliposomes (Wahrle, Das et al. 2002, Osenkowski, Ye et al. 2008, Kim, Kim et al. 2016), and γ-secretase activity has long been known to be pH-dependent (Li, Lai et al. 2000, Fraering, Ye et al. 2004, Quintero-Monzon, Martin et al. 2011, Maesako, Houser et al. 2022). The effects of these factors on all γ-secretase proteolytic processing steps and E-S complex stability are currently under investigation. We are also searching for compounds that rescue stalled complexes, as a potential therapeutic strategy for the prevention or treatment of AD.

Given the advantages of *C. elegans* as a model for neurodegenerative studies, future research may leverage these FAD models for genetic screening to identify mediators of synaptic dysfunction (Torres, Mira et al. 2025). Studies in *C. elegans* continue to highlight conserved molecular pathways that contribute to synapse abnormalities and the relevance of this model organism for investigating pathological mechanisms of AD (Van Pelt and Truttmann 2020, Alvarez, Alvarez-Illera et al. 2022, Xu, Kang et al. 2025) and FAD (Sarasija, Laboy et al. 2018, Ashkavand, Ryan et al. 2025). Revealing molecular mechanisms of pathogenesis in *C. elegans* neurodegenerative models would then justify much more difficult, lengthy and expensive studies in mammalian models and may ultimately lead to development of therapeutic agents for the prevention and treatment of Alzheimer's Disease. In this regard, the new *C. elegans* system described here may also provide a rapid and facile *in vivo* platform for AD drug discovery.

LIMITATIONS OF THE APPROACH

While the *C. elegans* model system described here has many advantages, we should point out important limitations to our approach. For instance, as the transgenes are expressed only in neurons, contributions due to FAD-mutant protein expression in other cell types, such as glial cells, cannot be observed. Also, because synaptic degeneration from neuronal expression of L166P PSEN1 in this model organism requires coexpression of exogenous substrate, the molecular mechanism may differ from that leading to synaptic degeneration in FAD. Furthermore, while we have clearly demonstrated the effects of the designed APP C99 mutations on processing of this substrate by human γ-secretase, testing whether these effects are recapitulated in *C. elegans* was not feasible. Because human PSEN1 is coexpressed, we believe it highly likely that processing occurs like it does in human cells. The critical interactions of substrate with γ-secretase essential for proteolytic processing are between substrate transmembrane domain and presenilin, the catalytic component (Yang, Zhou et al. 2019) (Zhou, Yang et al. 2019). Nevertheless, we cannot exclude that the mutant substrates are processed differently in *C. elegans*, even with human PSEN1, which must assemble with *C. elegans* orthologs of the other γ-secretase components. Finally, elevated APP C-terminal fragments such as C99 through inhibition of of γ-secretase activity can be neurotoxic (Kwart, Gregg et al. 2019) (Hung and Livesey 2018) (Bretou, Sannerud et al. 2024) (Im, Jiang et al. 2023) (Lauritzen, Pardossi-Piquard et al. 2016) (Lauritzen, Pardossi-Piquard et al. 2023) (Checler, Afram et al. 2021) (Vrancx and Annaert 2025). Expression of C99 is likely elevated in neurons in all of our models, but coexpression of WT C99 and WT PSEN1 does not lead to synaptic degeneration. Moreover, because of the slow turnover rate of γ-secretase and the low level of active enzyme (limited by endogenous subunits of the protease complex) make it unlikely that the introduced mutations further elevate C99 (Kamp, Winkler et al. 2015). Nevertheless, we cannot rule out that elevated C99 does not contribute at least partially to the observed synaptic degeneration.

METHODS

General workflow

Construction of *C. elegans* transgenes → Microinjection of transgenes in *C. elegans* hermaphrodite gonads → Selection of transformants → Phenotypic assays (lifespan analysis, brood size analysis, embryonic viability analysis, scoring of synaptic puncta using confocal microscopy).

C. elegans maintenance

All *C. elegans* strains used in the study were maintained at 15-22° C on nematode growth medium (NGM) plates seeded with *E. coli* (Brenner 1974). *juIs1* [*Punc-25*::SNB-1::GFP] was used as the parental strain to develop transgenic lines by injecting human C99 APP and/or PSEN1 or human C99 Notch and/or PSEN1 constructs along with co-injection marker *rol-6* (Kramer, French et al. 1990).

Cloning & molecular biology

Human C99APP and PS-1 cDNA were synthesized as described in a previous study (Devkota, Zhou et al. 2024). Similarly, human C99 Notch1 transgenes (wt and FF) were designed to include the following: 1) DNA encoding signal peptide (MLPGLALLLLAAWTARA) for membrane insertion, 2) coding sequence for 99 amino acids of Notch1 (wt and FF). These constructs were designed to include worm introns. All human constructs were cloned in worm expression vector pEVL415 (P*rgef-1*:*htau40::gfp::unc-54* 3′UTR) (Devkota, Zhou et al. 2024). Restriction digestion was performed using BamH1 and NgoM4 to linearize the vector. Plasmids harboring C99 wt Notch1 and C99 FF Notch1 sequences analogous to C99 APP constructs used in the previous study were synthesized using ‘GeneArt Gene Synthesis’ by ThermoFisher. These plasmids contain Kan^R genes for growth on bacterial plates and DNA extraction. The genes of interest were PCR amplified from the Thermofisher plasmids using primers that were designed to have ~ 15 bp 5’ extensions complementary to the 3’ sticky ends of the linearized vector. The fragments were PCR-purified and cloning was performed by In-Fusion cloning (TakaraBio) following manufacturer’s protocol. Ampicillin resistance allowed for specific isolation of bacterial clones containing Notch constructs. Clones were confirmed by PCR amplification and restriction digestion. In addition, plasmid DNA containing the gene inserts were validated by sequencing.

C. elegans transgenesis

The parental strain *juIs1* [*unc-25*p::*snb-1*::GFP + lin-15(+)] IV expresses GFP fused to synaptobrevin in presynaptic terminals of GABAergic DD and VD motor neurons and RME neurons (Hallam and Jin 1998). Human constructs with co-injection marker were microinjected into gonads of young adults of *juIs1* [*Punc-25*::SNB-1::GFP] to obtain transgenic lines. Injection mixes contain human APP (or Notch1) variant (8-10 ng/μl) and/or human PS-1 variant (8–10 ng/μl) and pRF4 (60.8 ng/μl) . Injection mixes for D257A PS1 contained 10ng/μl of DNA and pRF4 (60 ng/μl).

Plasmids used in the study are below. Full sequences of new transgenes are provided as a supplementary files Text S1, Text S2 and Text S3).

1. pEVL545 [*Prgef-1*:signal peptide : human wt C99APP :: *unc-54* 3'UTR]
2. pEVL546 [*Prgef-1*::signal peptide : human C99APP (I45F) :: *unc-5*4 3'UTR
3. pEVL547 [*Prgef-1*::signal peptide : human wt PS-1 :: *unc-54* 3'UTR]
4. pEVL548 [*Prgef-1*:: human L166P PS-1 :: *unc-54* 3'UTR]
5. pEVL549 [*Prgef-1*::signal peptide : human V44F I45F C99APP :: *unc-54* 3'UTR]
6. pEVL554 [*Prgef-1*::signal peptide : human V50F M51F C99APP :: *unc-54* 3'UTR]
7. pEVL555 [*Prgef-1*::signal peptide : human wt C99Notch :: *unc-54* 3'UTR] (Text S1)
8. pEVL556 [*Prgef-1*::signal peptide : human FF C99 Notch :: *unc-54* 3'UTR] (Text S2)
9. pEVL553 [P*rgef-1*:: human D257A PS-1 :: *unc-54* 3'UTR] (Text S3)

Strains generated in this study

wt C99APP + wt PS-1 Line 2	***lhEx662***
I45F C99APP + wt PS-1 Line 2	*lhEx656*
I45F C99APP Line 2	*lhEx649*
V44F I45F C99APP + wt PS-1 Line 2	*lhEx651*
V44F I45F C99APP Line 2	*lhEx653*
V50F M51F C99APP + wt PS-1 Line 2	*lhEx664*
wt C99APP + L166P PS-1 Line 2	*lhEx658*
L166P PS-1 Line 2	*lhEx660*
wt C99Notch1 + wt PS-1 Line 1	*lhEx669*
wt C99Notch1 + wt PS-1 Line 2	*lhEx671*
FF C99Notch1 + wt PS-1 Line 1	*lhEx672*
FF C99Notch1 + wt PS-1 Line 2	*lhEx673*
D257A PS-1 Line 1	*lhEx665*
D257A PS-1 Line 2	*lhEx666*
D257A PS-1 Line 3	*lhEx667*

Lifespan

L4 animals were isolated for lifespan experiments and maintained at 20 °C . To avoid contamination with progeny animals, adults were transferred to fresh plates whenever necessary. Plates were checked for live worms at least once in two days. Animals that did not move when prodded were considered dead. For D257A PSEN1 animals, L4 animals were also isolated and maintained at 20°C. Animals were plated in four technical replicates,

with each replicate containing 25 animals for an n-number of 100 animals. Animals were transferred to new plates everyday and scored for life. Animals that did not move when prodded were considered dead.

Microscopy and image analysis

L4 animals were transferred to fresh plates and were maintained at 20 ^{o}C. Day 1 to day 7 adults and day 9 adults were scored for the number of SNB-1::GFP puncta in the ventral and dorsal nerve cords. 0.5% 2-phenoxypropanol in M9 was used to anesthetize adult worms and those were mounted on 2% agarose pads for imaging. Imaging was done using Olympus FV1000 laser scanning confocal microscope at 60X magnification NA 1.42. All images were obtained processed and analyzed as described previously using GraphPad Prism 9 and 10 (Devkota, Zhou et al. 2024).

C. elegans were also imaged in the Microscopy and Analytical Imaging Resource Core Laboratory (RRID:SCR_021801) at The University of Kansas using a TCS SPE Laser Scanning Confocal Upright Microscope (Leica Microsystems, DM6-Q model), with the 488 nm laser line, a Leica 63X/1.3NA ACS APO oil objective, 12-bit spectral PMT detector and a Leica LAS X Imaging software (version 3.5.7.23225). Synaptic puncta signal was detected using 488 nm excitation, 500-520 nm emission range. Images were captured at 1024 x 1024-pixel resolution, no bidirectional scanning, and a zoom factor at 1.0.

Agarose Immobilization

For imaging of animals containing the D257A PS1 and L166P PS1 transgene, immobilization with agarose and polystyrene beads was used. L4 animals were transferred to fresh plates and maintained at 20°C. 10% agarose in M9 buffer was used to make the agarose pads. 1.5 uL of 0.1 um polystyrene beads (Sigma-Aldrich catalog 90517, Batch BCCL4220) were added to immobilize worms. Day 1, day 4, and day 7 adults were scored for the number of SNB-1::GFP puncta in the ventral and dorsal nerve cords in this manner. All control animals were also scored using this method and compared against D257A and L166P mutants. Image instrumentation and analysis was the same as all other lines imaged under anesthetization using the Olympus FV1000.

Brood size & Embryonic Viability Assays

To analyze the brood size, on day 1, one L4 hermaphrodite was transferred to each plate. The worms were allowed to develop into adults and lay eggs for 24 hours at 20 °C, after which the adult worm was transferred to a new plate on day 2. It was ensured that no eggs or other worms were transferred inadvertently. On day 3, the day 1 plate was scored separately for L1 larvae and unhatched eggs. This process was repeated until day 5 when the adult worm was removed and day 7 when the last scoring was recorded for day 5 plates (Hornsten, Lieberthal et al. 2007, Gallrein, Iburg et al. 2021).

Data analysis

Lifespan: Plotting of survival curves, calculation of median lifespan and statistical analysis were performed in ‘Sigmaplot’ using Kaplan Meier (log-rank test) method. Pairwise

comparisons were made using Holm-Sidak method with a significance cutoff of $p<0.05$. All pairwise comparisons are shown in Tables S1–7).

Microscopic image analysis: All confocal image processing and analysis were performed using Fiji (ImageJ) software, as described in our previous report (Devkota, Zhou et al. 2024). In brief, L4 animals were selected and maintained at 20°C, then imaged on different days of adulthood ranging from day 1 through day 9 for synaptobrevin GFP-expressing puncta on both dorsal and ventral nerve cords. Images were then analyzed using Fiji (ImageJ) software. Fluorescent confocal images were stacked in the Z plane and converted to a binary image so that a threshold to identify each puncta could be determined. Puncta were referenced to the original binary image to make sure all puncta were acquired. Particles within the desired size range were measured and the location of the puncta by (x,y) coordinates was the output in the software. The average number of synaptic puncta in 100 μm was calculated from the distances between two puncta on the x-axis. Collection of the output was placed in Microsoft Excel, and graph generation and statistical analysis was conducted in GraphPad Prism 9 software. ANOVA was conducted for all days collected between and within strains and Tukey's post-hoc analysis was used to determine significance for all pair-wise comparisons. For all multiple comparisons statistical tests, a threshold of significance was set at $p<0.05$. Specifics of statistical testing are in figure legends and in Supplemental Information Tables S8 and S9. Significance depicted on graphs was determined by what comparisons showed significance (i.e., if between strains on different days showed significance versus within strain on different days showed significance). Non-significant comparisons were not always shown on graphs, but are indicated in figure legends.

Brood size & embryonic viability: Brood size for each replicate of a given strain is the sum of total progeny including unhatched embryos (along with live larvae) from each parent hermaphrodite, obtained by summing the daily counts from day 1 to day 5.

Brood size = Live progeny + unhatched embryo.

Embryonic viability percentage was calculated for each biological replicate of a given strain The numbers of live progeny and unhatched embryos are obtained by totaling the daily count across the experimental period (Kwah and Jaramillo-Lambert 2023).

Embryonic viability = [Total live progeny/ (Total live progeny + Total unhatched embryo)] × 100

In both cases, statistical analysis was performed in GraphPad Prism using one way ANOVA test (Dunnett's multiple comparisons test). Comparisons were made with *juIs1* with $p>0.05$ ns, $p\leq 0.05$ *, $p\leq 0.01$ **, $p\leq 0.001$ ***, $p< 0.0001$ ****.

Supplementary Material

Refer to Web version on PubMed Central for supplementary material.

Acknowledgment:

We thank E. Lundquist (U. Kansas) for injection apparatus for microinjection of transgenes into *C. elegans*, and E. Rosa-Molinar and N. Martinez-Rivera for confocal microscopy images obtained at the Microscopy and Analytical Imaging Research Resource Core Laboratory at U. Kansas. This work was supported by grants AG66986 and AG79569 from the US National Institutes of Health and a Pilot Project Grant from the University of Kansas Alzheimer Disease Research Center via NIH grant P30 AG072973.

REFERENCES

Adamla F and Ignatova Z (2015). “Somatic expression of unc-54 and vha-6 mRNAs declines but not pan-neuronal rgef-1 and unc-119 expression in aging Caenorhabditis elegans.” Sci Rep 5: 10692. [PubMed: 26031360]

Alvarez J, Alvarez-Illera P, Santo-Domingo J, Fonteriz RI and Montero M (2022). “Modeling Alzheimer’s Disease in Caenorhabditis elegans.” Biomedicines 10(2).

Arafi P, Devkota S, Williams E, Maesako M and Wolfe MS (2025). “Alzheimer-mutant γ-secretase complexes stall amyloid β-peptide production.” Elife 13: RP102274. [PubMed: 39932776]

Ashkavand Z, Ryan KC, Laboy JT, Patel R, Geller B and Norman KR (2025). “Identification of presenilin mutations that have sufficient gamma-secretase proteolytic activity to mediate Notch signaling but disrupt organelle and neuronal health.” Neurobiol Dis 212: 106961. [PubMed: 40404063]

Bateman RJ, Aisen PS, De Strooper B, Fox NC, Lemere CA, Ringman JM, Salloway S, Sperling RA, Windisch M and Xiong C (2011). “Autosomal-dominant Alzheimer’s disease: a review and proposal for the prevention of Alzheimer’s disease.” Alzheimers Res Ther 3(1): 1. [PubMed: 21211070]

Bieschke J, Cohen E, Murray A, Dillin A and Kelly JW (2009). “A kinetic assessment of the C. elegans amyloid disaggregation activity enables uncoupling of disassembly and proteolysis.” Protein Sci 18(11): 2231–2241. [PubMed: 19701939]

Bolduc DM, Montagna DR, Seghers MC, Wolfe MS and Selkoe DJ (2016). “The amyloid-beta forming tripeptide cleavage mechanism of gamma-secretase.” Elife 5.

Breijyeh Z and Karaman R (2020). “Comprehensive Review on Alzheimer’s Disease: Causes and Treatment.” Molecules 25(24).

Brenner S (1974). “The genetics of Caenorhabditis elegans.” Genetics 77(1): 71–94. [PubMed: 4366476]

Bretou M, Sannerud R, Escamilla-Ayala A, Leroy T, Vrancx C, Van Acker ZP, Perdok A, Vermeire W, Vorsters I, Van Keymolen S, Maxson M, Pavie B, Wierda K, Eskelinen EL and Annaert W (2024). “Accumulation of APP C-terminal fragments causes endolysosomal dysfunction through the dysregulation of late endosome to lysosome-ER contact sites.” Dev Cell 59(12): 1571–1592 e1579. [PubMed: 38626765]

Brou C, Logeat F, Gupta N, Bessia C, LeBail O, Doedens JR, Cumano A, Roux P, Black RA and Israël A (2000). “A Novel Proteolytic Cleavage Involved in Notch Signaling: The Role of the Disintegrin-Metalloprotease TACE.” Molecular Cell 5: 207–216. [PubMed: 10882063]

Cai Q and Tammineni P (2017). “Mitochondrial Aspects of Synaptic Dysfunction in Alzheimer’s Disease.” J Alzheimers Dis 57(4): 1087–1103. [PubMed: 27767992]

Cardillo G (2006). “Holm-Sidak t-test: a routine for multiple t-test comparisons.” from https://github.com/dnafinder/holm.

Checler F, Afram E, Pardossi-Piquard R and Lauritzen I (2021). “Is gamma-secretase a beneficial inactivating enzyme of the toxic APP C-terminal fragment C99?” J Biol Chem 296: 100489. [PubMed: 33662398]

Chen L, Fu Y, Ren M, Xiao B and Rubin CS (2011). “A RasGRP, C. elegans RGEF-1b, couples external stimuli to behavior by activating LET-60 (Ras) in sensory neurons.” Neuron 70(1): 51–65. [PubMed: 21482356]

DeKosky ST and Scheff SW (1990). “Synapse loss in frontal cortex biopsies in Alzheimer’s disease: correlation with cognitive severity.” Ann Neurol 27(5): 457–464. [PubMed: 2360787]

Devkota S, Maesako M and Wolfe MS (2025). “Presenilin-1 Familial Alzheimer Mutations Impair γ-Secretase Cleavage of APP Through Stabilized Enzyme–Substrate Complex Formation.” Biomolecules 15: 955. [PubMed: 40723827]

Devkota S, Williams TD and Wolfe MS (2021). “Familial Alzheimer’s disease mutations in amyloid protein precursor alter proteolysis by γ-secretase to increase amyloid β-peptides of >45 residues.” J Biol Chem. 296:100281.(doi): 10.1016/j.jbc.2021.100281. [PubMed: 33450230]

Devkota S, Zhou R, Nagarajan V, Maesako M, Do H, Noorani A, Overmeyer C, Bhattarai S, Douglas JT, Saraf A, Miao Y, Ackley BD, Shi Y and Wolfe MS (2024). “Familial Alzheimer mutations stabilize synaptotoxic gamma-secretase-substrate complexes.” Cell Rep 43(2): 113761. [PubMed: 38349793]

Devkota S, Zhou R, Nagarajan V, Maesako M, Do H, Noorani A, Overmeyer C, Bhattarai S, Douglas JT, Saraf A, Miao Y, Ackley BD, Shi Y and Wolfe MS (2024). “Familial Alzheimer mutations stabilize synaptotoxic γ-secretase-substrate complexes.” Cell Rep 43(2): 113761. [PubMed: 38349793]

Fraering PC, Ye W, Strub JM, Dolios G, LaVoie MJ, Ostaszewski BL, Van Dorsselaer A, Wang R, Selkoe DJ and Wolfe MS (2004). “Purification and Characterization of the Human gamma-Secretase Complex.” Biochemistry 43(30): 9774–9789. [PubMed: 15274632]

Gallrein C, Iburg M, Michelberger T, Kocak A, Puchkov D, Liu F, Ayala Mariscal SM, Nayak T, Kaminski Schierle GS and Kirstein J (2021). “Novel amyloid-beta pathology C. elegans model reveals distinct neurons as seeds of pathogenicity.” Prog Neurobiol 198: 101907. [PubMed: 32926945]

Goate A, Chartier-Harlin MC, Mullan M, Brown J, Crawford F, Fidani L, Giuffra L, Haynes A, Irving N, James L and et al. (1991). “Segregation of a missense mutation in the amyloid precursor protein gene with familial Alzheimer’s disease.” Nature 349(6311): 704–706. [PubMed: 1671712]

Güner G and Lichtenthaler SF (2020). “The substrate repertoire of γ-secretase/presenilin.” Semin Cell Dev Biol 105: 27–42. [PubMed: 32616437]

Hallam SJ and Jin Y (1998). “lin-14 regulates the timing of synaptic remodelling in Caenorhabditis elegans.” Nature 395(6697): 78–82. [PubMed: 9738501]

Hornsten A, Lieberthal J, Fadia S, Malins R, Ha L, Xu X, Daigle I, Markowitz M, O’Connor G, Plasterk R and Li C (2007). “APL-1, a Caenorhabditis elegans protein related to the human beta-amyloid precursor protein, is essential for viability.” Proc Natl Acad Sci U S A 104(6): 1971–1976. [PubMed: 17267616]

Hung COY and Livesey FJ (2018). “Altered gamma-Secretase Processing of APP Disrupts Lysosome and Autophagosome Function in Monogenic Alzheimer’s Disease.” Cell Rep 25(13): 3647–3660 e3642. [PubMed: 30590039]

Hunter P (2024). “The controversy around anti-amyloid antibodies for treating Alzheimer’s disease : The European Medical Agency’s ruling against the latest anti-amyloid drugs highlights the ongoing debate about their safety and efficacy.” EMBO Rep.

Im E, Jiang Y, Stavrides PH, Darji S, Erdjument-Bromage H, Neubert TA, Choi JY, Wegiel J, Lee JH and Nixon RA (2023). “Lysosomal dysfunction in Down syndrome and Alzheimer mouse models is caused by v-ATPase inhibition by Tyr(682)-phosphorylated APP betaCTF.” Sci Adv 9(30): eadg1925. [PubMed: 37494443]

Kamp F, Winkler E, Trambauer J, Ebke A, Fluhrer R and Steiner H (2015). “Intramembrane proteolysis of beta-amyloid precursor protein by gamma-secretase is an unusually slow process.” Biophys J 108(5): 1229–1237. [PubMed: 25762334]

Kim Y, Kim C, Jang HY and Mook-Jung I (2016). “Inhibition of Cholesterol Biosynthesis Reduces γ-Secretase Activity and Amyloid-β Generation.” J Alzheimers Dis 51(4): 1057–1068. [PubMed: 26923021]

Kramer JM, French RP, Park EC and Johnson JJ (1990). “The Caenorhabditis elegans rol-6 gene, which interacts with the sqt-1 collagen gene to determine organismal morphology, encodes a collagen.” Mol Cell Biol 10(5): 2081–2089. [PubMed: 1970117]

Krstic D and Knuesel I (2013). “Deciphering the mechanism underlying late-onset Alzheimer disease.” Nat Rev Neurol 9(1): 25–34. [PubMed: 23183882]

Kurkinen M, Fulek M, Fulek K, Beszlej JA, Kurpas D and Leszek J (2023). “The Amyloid Cascade Hypothesis in Alzheimer’s Disease: Should We Change Our Thinking?” Biomolecules 13(3).

Kwah JK and Jaramillo-Lambert A (2023). “Measuring Embryonic Viability and Brood Size in Caenorhabditis elegans.” J Vis Exp(192).

Kwart D, Gregg A, Scheckel C, Murphy EA, Paquet D, Duffield M, Fak J, Olsen O, Darnell RB and Tessier-Lavigne M (2019). “A Large Panel of Isogenic APP and PSEN1 Mutant Human iPSC Neurons Reveals Shared Endosomal Abnormalities Mediated by APP beta-CTFs, Not Abeta.” Neuron 104(2): 256–270 e255. [PubMed: 31416668]

Lauritzen I, Pardossi-Piquard R, Bourgeois A, Pagnotta S, Biferi MG, Barkats M, Lacor P, Klein W, Bauer C and Checler F (2016). “Intraneuronal aggregation of the beta-CTF fragment of APP (C99) induces Abeta-independent lysosomal-autophagic pathology.” Acta Neuropathol 132(2): 257–276. [PubMed: 27138984]

Lauritzen I, Pardossi-Piquard R, Bourgeois A, Pagnotta S, Biferi MG, Barkats M, Lacor P, Klein W, Bauer C and Checler F (2023). “Correction to: Intraneuronal aggregation of the beta−CTF fragment of APP (C99) induces Abeta−independent lysosomal-autophagic pathology.” Acta Neuropathol 146(4): 659–660. [PubMed: 37540291]

Levitan D, Doyle TG, Brousseau D, Lee MK, Thinakaran G, Slunt HH, Sisodia SS and Greenwald I (1996). “Assessment of normal and mutant human presenilin function in Caenorhabditis elegans.” Proc Natl Acad Sci U S A 93(25): 14940–14944. [PubMed: 8962160]

Levitan D and Greenwald I (1995). “Facilitation of lin-12-mediated signalling by sel-12, a Caenorhabditis elegans S182 Alzheimer’s disease gene.” Nature 377(6547): 351–354. [PubMed: 7566091]

Li YM, Lai MT, Xu M, Huang Q, DiMuzio-Mower J, Sardana MK, Shi XP, Yin KC, Shafer JA and Gardell SJ (2000). “Presenilin 1 is linked with gamma-secretase activity in the detergent solubilized state.” Proc Natl Acad Sci U S A 97(11): 6138–6143. [PubMed: 10801983]

Link CD (1995). “Expression of human beta-amyloid peptide in transgenic Caenorhabditis elegans.” Proc Natl Acad Sci U S A 92(20): 9368–9372. [PubMed: 7568134]

Maesako M, Houser MCQ, Turchyna Y, Wolfe MA-O and Berezovska O (2022). “Presenilin/γ-Secretase Activity Is Located in Acidic Compartments of Live Neurons.” J Neurosci 42(1): 145–154. [PubMed: 34810230]

Makin S (2018). “The amyloid hypothesis on trial.” Nature 559(7715): S4–S7. [PubMed: 30046080]

Malvankar SR and Wolfe MS (2025). “Effects of Transmembrane Phenylalanine Residues on gamma-Secretase-Mediated Notch-1 Proteolysis.” ACS Chem Neurosci 16(5): 844–855. [PubMed: 39950614]

Malvankar SR and Wolfe MS (2025). “Effects of Transmembrane Phenylalanine Residues on γ-Secretase-Mediated Notch-1 Proteolysis.” ACS Chem Neurosci 16(5): 844–855. [PubMed: 39950614]

McColl G, Roberts BR, Gunn AP, Perez KA, Tew DJ, Masters CL, Barnham KJ, Cherny RA and Bush AI (2009). “The Caenorhabditis elegans A beta 1–42 model of Alzheimer disease predominantly expresses A beta 3–42.” J Biol Chem 284(34): 22697–22702. [PubMed: 19574211]

McColl G, Roberts BR, Pukala TL, Kenche VB, Roberts CM, Link CD, Ryan TM, Masters CL, Barnham KJ, Bush AI and Cherny RA (2012). “Utility of an improved model of amyloid-beta (Abeta(1)(−)(4)(2)) toxicity in Caenorhabditis elegans for drug screening for Alzheimer’s disease.” Mol Neurodegener 7: 57. [PubMed: 23171715]

Merritt C, Rasoloson D, Ko D and Seydoux G (2008). “3’ UTRs are the primary regulators of gene expression in the C. elegans germline.” Curr Biol 18(19): 1476–1482. [PubMed: 18818082]

Morris JC, Weiner M, Xiong C, Beckett L, Coble D, Saito N, Aisen PS, Allegri R, Benzinger TLS, Berman SB, Cairns NJ, Carrillo MC, Chui HC, Chhatwal JP, Cruchaga C, Fagan AM, Farlow M, Fox NC, Ghetti B, Goate AM, Gordon BA, Graff-Radford N, Day GS, Hassenstab J, Ikeuchi T, Jack CR, Jagust WJ, Jucker M, Levin J, Massoumzadeh P, Masters CL, Martins R, McDade E, Mori H, Noble JM, Petersen RC, Ringman JM, Salloway S, Saykin AJ, Schofield PR, Shaw LM, Toga AW, Trojanowski JQ, Vöglein J, Weninger S, Bateman RJ and Buckles VD (2022). “Autosomal dominant and sporadic late onset Alzheimer’s disease share a common in vivo pathophysiology.” Brain 145(10): 3594–3607. [PubMed: 35580594]

Mumm JS, Schroeter EH, Saxena MT, Griesemer A, Tian X, Pan DJ, Ray WJ and Kopan R (2000). "A Ligand-Induced Extracellular Cleavage Regulates Gamma-Secretase-like Proteolytic Activation of Notch1." Molecular Cell 5: 197–206. [PubMed: 10882062]

Munoz-Jimenez C, Ayuso C, Dobrzynska A, Torres-Mendez A, Ruiz PC and Askjaer P (2017). "An Efficient FLP-Based Toolkit for Spatiotemporal Control of Gene Expression in Caenorhabditis elegans." Genetics 206(4): 1763–1778. [PubMed: 28646043]

Osenkowski P, Ye W, Wang R, Wolfe MS and Selkoe DJ (2008). "Direct and potent regulation of gamma-secretase by its lipid microenvironment." J Biol Chem 283(33): 22529–22540. [PubMed: 18539594]

Pelucchi S, Gardoni F, Di Luca M and Marcello E (2022). "Synaptic dysfunction in early phases of Alzheimer's Disease." Handb Clin Neurol 184: 417–438. [PubMed: 35034752]

Pope CA, Wilkins HM, Swerdlow RH and Wolfe MS (2021). "Mutations in the Amyloid-beta Protein Precursor Reduce Mitochondrial Function and Alter Gene Expression Independent of 42-Residue Amyloid-beta Peptide." J Alzheimers Dis 83(3): 1039–1049. [PubMed: 34366346]

Quintero-Monzon O, Martin MM, Fernandez MA, Cappello CA, Krzysiak AJ, Osenkowski P and Wolfe MS (2011). "Dissociation between the processivity and total activity of gamma-secretase: implications for the mechanism of Alzheimer's disease-causing presenilin mutations." Biochemistry 50(42): 9023–9035. [PubMed: 21919498]

Sarasija S, Laboy JT, Ashkavand Z, Bonner J, Tang Y and Norman KR (2018). "Presenilin mutations deregulate mitochondrial Ca(2+) homeostasis and metabolic activity causing neurodegeneration in Caenorhabditis elegans." Elife 7: e33052. [PubMed: 29989545]

Sherrington R, Rogaev EI, Liang Y, Rogaeva EA, Levesque G, Ikeda M, Chi H, Lin C, Li G, Holman K, Tsuda T, Mar L, Foncin JF, Bruni AC, Montesi MP, Sorbi S, Rainero I, Pinessi L, Nee L, Chumakov I, Pollen D, Brookes A, Sanseau P, Polinsky RJ, Wasco W, Da Silva HA, Haines JL, Perkicak-Vance MA, Tanzi RE, Roses AD, Fraser PE, Rommens JM and St George-Hyslop PH (1995). "Cloning of a gene bearing missense mutations in early-onset familial Alzheimer's disease." Nature 375(6534): 754–760. [PubMed: 7596406]

Subramanian J, Savage JC and Tremblay ME (2020). "Synaptic Loss in Alzheimer's Disease: Mechanistic Insights Provided by Two-Photon in vivo Imaging of Transgenic Mouse Models." Front Cell Neurosci 14: 592607. [PubMed: 33408613]

Takami M, Nagashima Y, Sano Y, Ishihara S, Morishima-Kawashima M, Funamoto S and Ihara Y (2009). "gamma-Secretase: successive tripeptide and tetrapeptide release from the transmembrane domain of beta-carboxyl terminal fragment." J Neurosci 29(41): 13042–13052. [PubMed: 19828817]

Tanzi RE (2012). "The genetics of Alzheimer disease." Cold Spring Harb Perspect Med 2(10): pii: a006296. [PubMed: 23028126]

Torres AK, Mira RG, Pinto C and Inestrosa NC (2025). "Studying the mechanisms of neurodegeneration: C. elegans advantages and opportunities." Front Cell Neurosci 19: 1559151. [PubMed: 40207239]

Treusch S, Hamamichi S, Goodman JL, Matlack KE, Chung CY, Baru V, Shulman JM, Parrado A, Bevis BJ, Valastyan JS, Han H, Lindhagen-Persson M, Reiman EM, Evans DA, Bennett DA, Olofsson A, DeJager PL, Tanzi RE, Caldwell KA, Caldwell GA and Lindquist S (2011). "Functional links between Abeta toxicity, endocytic trafficking, and Alzheimer's disease risk factors in yeast." Science 334(6060): 1241–1245. [PubMed: 22033521]

Van Pelt KM and Truttmann MC (2020). "Caenorhabditis elegans as a model system for studying aging-associated neurodegenerative diseases." Transl Med Aging 4: 60–72. [PubMed: 34327290]

Vrancx C and Annaert W (2025). "Amyloid precursor protein carboxy-terminal fragments as catalyzers of endolysosomal dysfunction in Alzheimer's disease." Trends Neurosci 48(7): 538–551. [PubMed: 40506325]

Wahrle S, Das P, Nyborg AC, McLendon C, Shoji M, Kawarabayashi T, Younkin LH, Younkin SG and Golde TE (2002). "Cholesterol-dependent gamma-secretase activity in buoyant cholesterol- rich membrane microdomains." Neurobiol Dis 9(1): 11–23. [PubMed: 11848681]

Wang B, Yang W, Wen W, Sun J, Su B, Liu B, Ma D, Lv D, Wen Y, Qu T, Chen M, Sun M, Shen Y and Zhang X (2010). “Gamma-secretase gene mutations in familial acne inversa.” Science 330(6007): 1065. [PubMed: 20929727]

Wolfe MS (2025). “Presenilin, γ-Secretase, and the Search for Pathogenic Triggers of Alzheimer’s Disease.” Biochemistry 64(8): 1662–1672. [PubMed: 39996369]

Xu R, Kang Q, Yang X, Yi P and Zhang R (2025). “Unraveling Molecular Targets for Neurodegenerative Diseases Through Caenorhabditis elegans Models.” Int J Mol Sci 26(7).

Yan K, Zhang C, Kang J, Montenegro P and Shen J (2024). “Cortical neurodegeneration caused by Psen1 mutations is independent of Abeta.” Proc Natl Acad Sci U S A 121(34): e2409343121. [PubMed: 39136994]

Yang G, Zhou R, Zhou Q, Guo X, Yan C, Ke M, Lei J and Shi Y (2019). “Structural basis of Notch recognition by human gamma-secretase.” Nature 565(7738): 192–197. [PubMed: 30598546]

Zhang H, Ma Q, Zhang YW and Xu H (2012). “Proteolytic processing of Alzheimer’s beta-amyloid precursor protein.” J Neurochem 120 Suppl 1(Suppl 1): 9–21. [PubMed: 22122372]

Zhou R, Yang G, Guo X, Zhou Q, Lei J and Shi Y (2019). “Recognition of the amyloid precursor protein by human gamma-secretase.” Science 363(6428).

Highlights

1. Stalled γ-secretase enzyme-substrate complexes per se can trigger synaptic loss.
2. Notch substrate can replace APP substrate to induce synaptic loss.
3. Proteolytically inactive presenilin alone does not trigger synaptic loss.

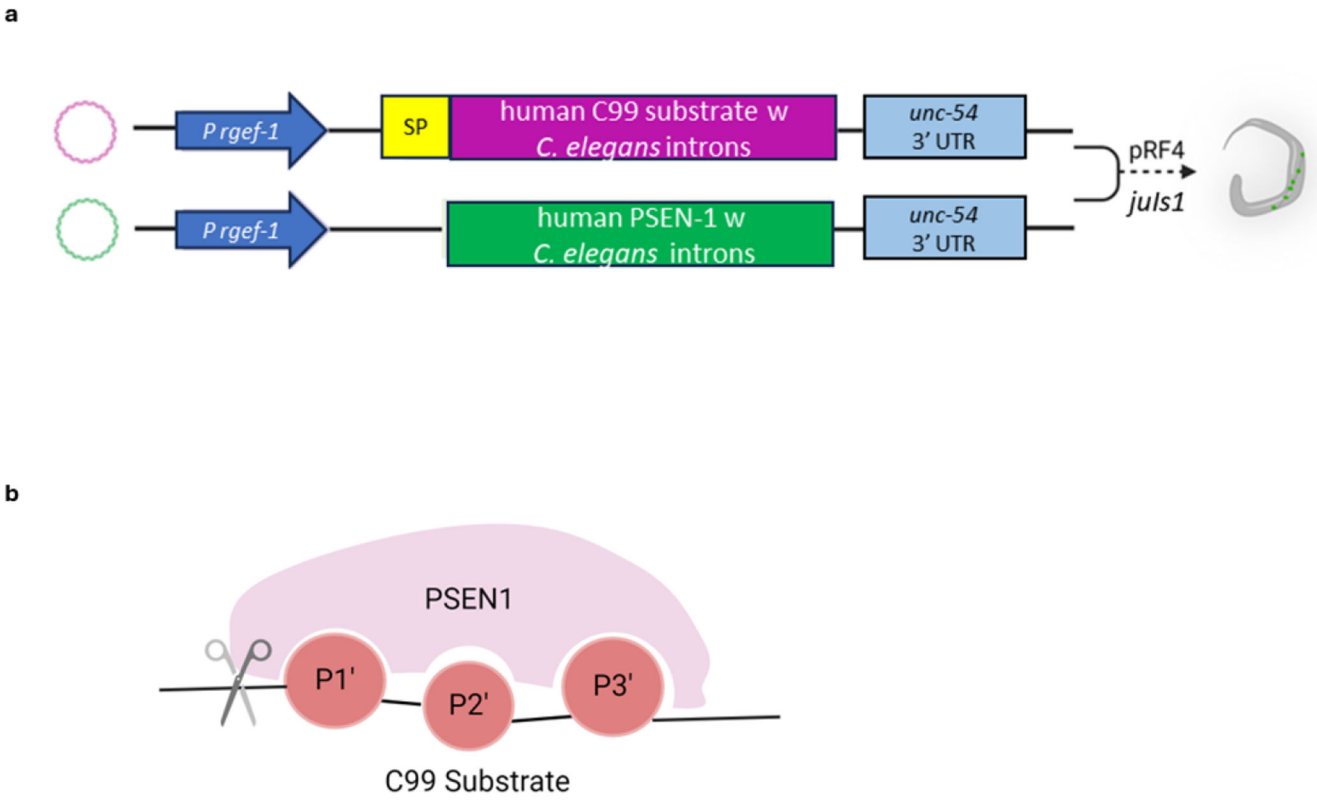

Figure 1. Design and creation of transgenic *C. elegans*.

a. **Schematic of transgenic *C. elegans* vectors.** Transgenic *C. elegans* lines were obtained by microinjection of either or combination of human PSEN-1 (also called PS-1) and human C99 substrate (APP or Notch-1) driven by pan-neuronal *rgef-1* promoter into the parental line *juIs1. rol-6* (dominant roller marker) expressed in pRF-4 plasmid was used as the co-injection marker to select for transformants. This results in transformant *C. elegans* that are roller worms having synaptic puncta marked by GFP- tagged synaptobrevin along the nerve cord.

b. **Visual representation of substrate processing by PSEN-1.** PSEN-1 proteolyzes substrates by initial endoproteolysis followed by processive tripeptide trimming. P1', P2' and P3' are amino acids of the substrate accommodated in three corresponding active-site pockets in PSEN-1.

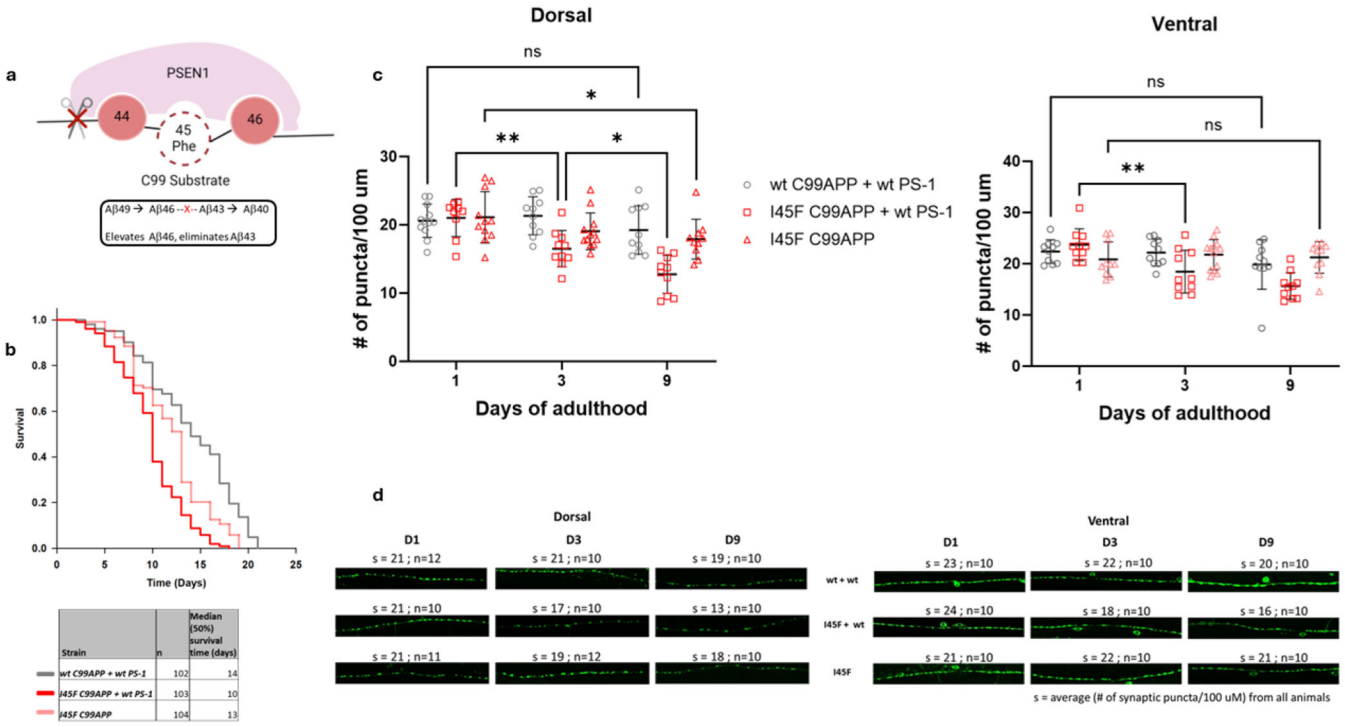

Figure 2. wt PS-1 exacerbates FAD-mutant I45F C99-induced synaptic loss in *C. elegans*.

a. **Visual representation of I45F C99APP processing by PSEN-1.** C99APP has a Phe substitution in the P2' position of the cleavage site preventing the formation of Aβ43.

b. **Shorter lifespan of I45F C99APP + wt PS-1 animals.** Kaplan-Meier curves of 'n' animals show the fraction of animals alive on different days. Ages of control animals - wt C99APP + wt PS-1 and I45F C99APP at median survival were 14 & 13 days respectively, while that of I45F C99APP + wt PS-1 was significantly shorter (10 days).

c. **Age-dependent loss of synaptic puncta in I45F C99APP + wt PS-1 animals.** The average number of synaptic puncta per 100 μm in 'n' transgenic worms for each day is shown in the scatter plots for dorsal and ventral cords. The scatter plot displays all individual data points. Superimposed on the data are the mean values represented by the horizontal lines, with vertical bars indicating the standard deviation (SD). The 'n' for each day for a given mutant can be found in panel d. The number of synaptic puncta in I45F C99APP + wt PS-1 reduced on day 3 compared to day 1 significantly in dorsal nerve cord, while loss of synaptic puncta in I45F C99APP animals was first seen later, on day 9. ($p>0.05$ ns, $p\leq 0.05$ *, $p\leq 0.01$ **, $p\leq 0.001$ ***, $p< 0.0001$ ****). Similarly, in ventral nerve cord, synaptic density in I45F C99APP + wt PS-1 reduced significantly on day 3 compared to day 1 but no significant reduction in the same was seen in either control. Note that in order to simplify visualization, data is plotted and statistics noted to indicate the earliest days on which significant differences occurred.

d. **Age-dependent loss of synaptic puncta in I45F C99APP + wt PS-1 animals.** 100 μm sections of representative confocal images for wildtype (1st row) and transgenic animals are shown for days 1, 3 and 9 for dorsal (left) and ventral (right). 's' denotes the average of (number of synaptic puncta per 100 μm) from 'n' animals. In I45 C99APP + wt PS-1 dorsal nerve cord, on day 3, s value dropped to17, compared to s=21 on day 1. Similarly, the value

of s dropped to 18 on day 3 compared to 24 on day 1 in ventral nerve. Note the gaps in synaptic puncta in these images, increasing the distance between two consecutive puncta.

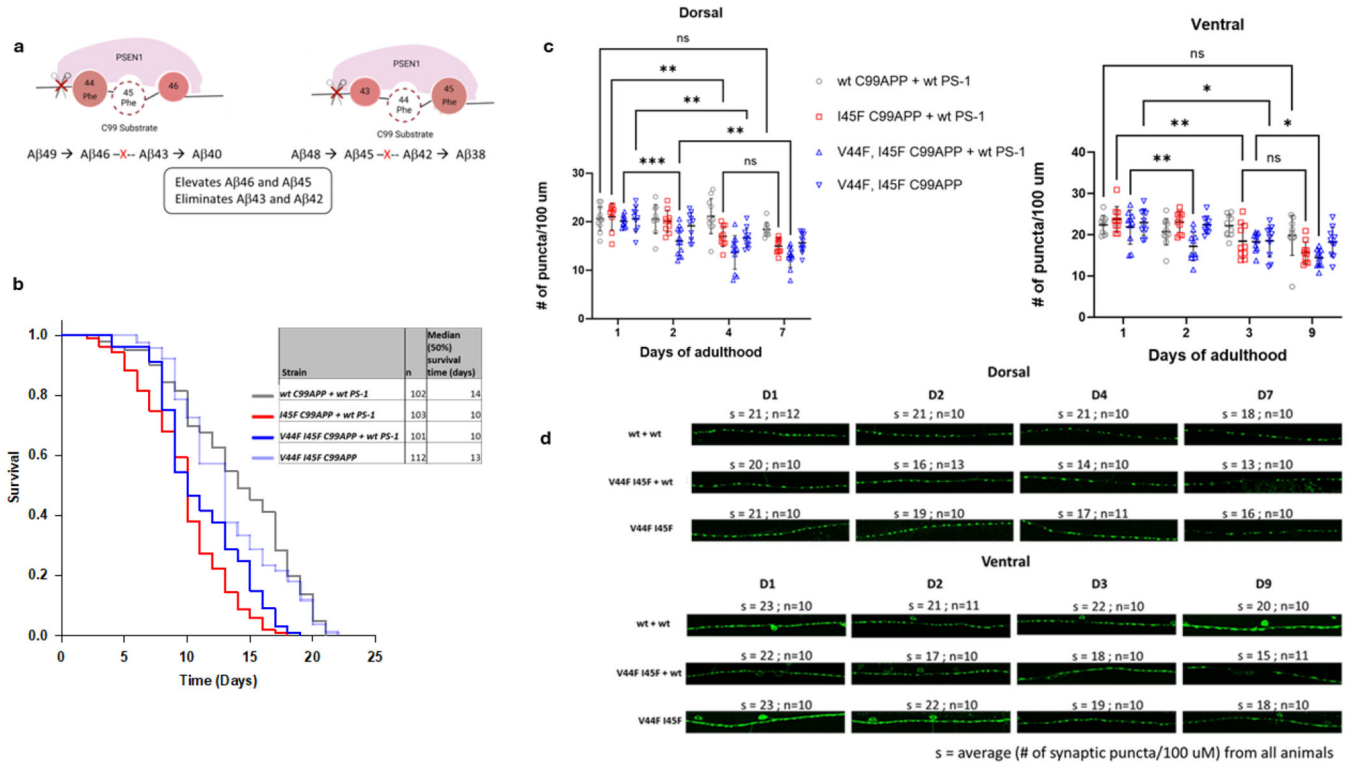

Figure 3. Synaptic loss is triggered independently of Aβ42.

a. **Visual representation of V44F/I45F C99APP processing by PSEN-1.** C99APP has two Phe substitutions in the P2' positions each along Aβ40 and Aβ42 pathways preventing the formation of Aβ43 and Aβ42.

b. **Shorter lifespan of V44F/I45F C99APP + wt PS-1 animals.** Kaplan-Meier curves of 'n' animals show the fraction of animals alive on different days. The ages of control animals (wt C99APP + wt PS-1 and V44F I45F C99APP) at median survival were 14 and 13 days respectively, while that of V44F I45F C99APP + wt PS-1 was significantly shorter (10 days).

c. **Age-dependent loss of synaptic puncta in V44F/I45F C99APP + wt PS-1 animals.** The average number of synaptic puncta per 100 μm in 'n' transgenic worms for each day is shown in the scatter plots for dorsal and ventral cords. The scatter plot displays all individual data points. Superimposed on the data are the mean values represented by the horizontal lines, with vertical bars indicating the standard deviation (SD). The 'n' for each day for a given mutant can be found in panel d. In the dorsal nerve cord, the number of synaptic puncta in V44F/I45F C99APP + wt PS-1 reduced significantly on day 2 compared to day 1 and then again on day 7, while significant loss of synaptic puncta in control V44F/I45F C99APP first occurred later on day 4. In the ventral nerve cord, loss of synaptic puncta in V44F/I45F C99APP + wt PS-1 first occurred on day 2 compared to day 1, while such loss was first seen later, on day 3, in V44F I45F C99APP animals. In control wt C99APP + wt PS-1 and in FAD mutant I45F C99APP + wt PS-1, loss of synaptic puncta occurred later in dorsal and ventral nerves than that in V44F/I45F C99APP + PS-1 mutant. ($p>0.05$ ns, $p\leq 0.05$ *, $p\leq 0.01$ **, $p\leq 0.001$ ***, $p< 0.0001$ ****). Note that in order to simplify

visualization, data is plotted and statistics noted to indicate the earliest days on which significant differences occurred.

d. **Age-dependent loss of synaptic puncta in V44F/I45F C99APP + wt PS-1 animals.** 100 μm sections of representative confocal images for wildtype (1st row) and transgenic animals are shown for days 1, 2, 4 and 7 for dorsal (left) and days 1, 2, 3 and 9 for ventral (right). 's' denotes the average of (number of synaptic puncta per 100 μm) from 'n' animals. In V44F/I45 C99APP + wt PS-1 dorsal nerve cord, on day 2, s value dropped significantly to 16, compared to s=20 on day 1. Similarly, the value of s dropped significantly to 17 on day 2 compared to 22 on day 1 in ventral nerve. Note the gaps in synaptic puncta in these images, increasing the distance between two consecutive puncta.

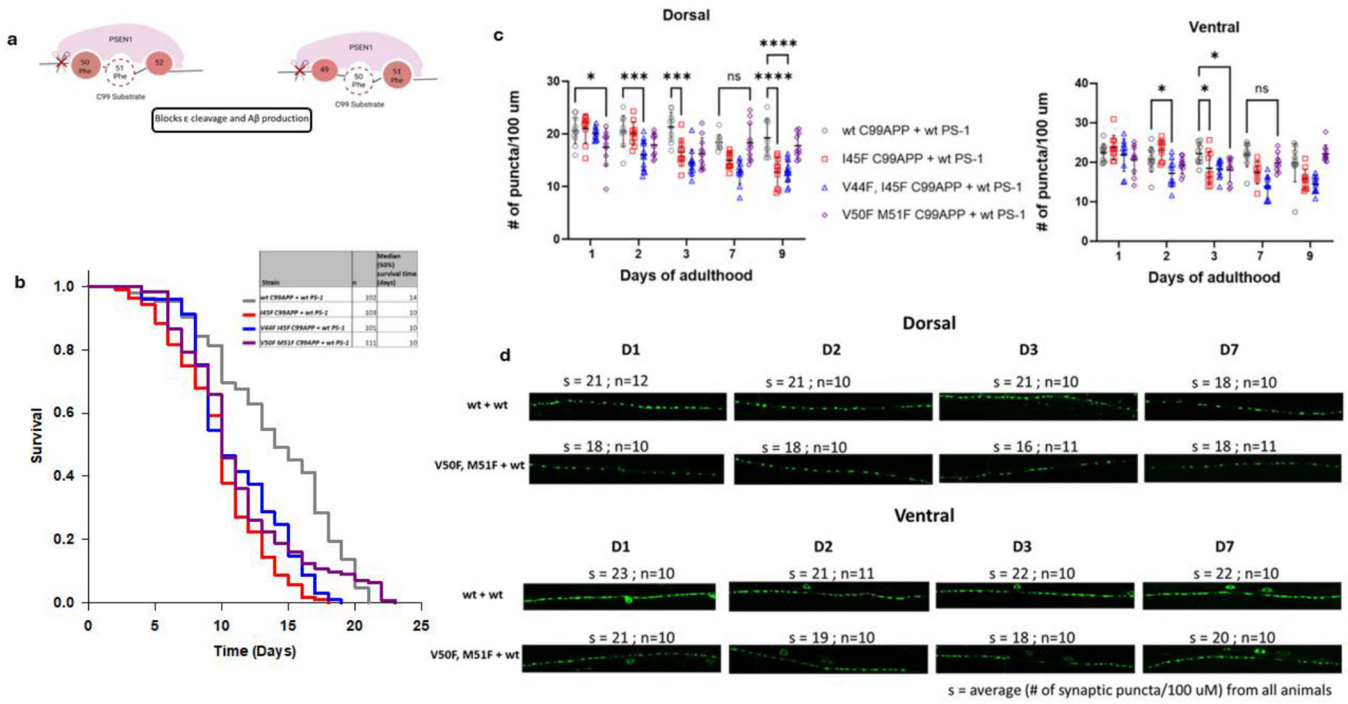

Figure 4. Synaptic loss is triggered independently of Aβ.

a. **Visual representation of V50F/M51F C99APP processing by PSEN-1.** C99APP has two Phe substitutions in the P2' positions relative to initial endoproteolysis (ε) sites for both the Aβ40 and Aβ42 pathways, preventing the formation of Aβ production.

b. **Shortened lifespan of V50F/M51F C99APP + wt PS-1 animals.** Kaplan-Meier curves of 'n' animals show the fraction of animals alive at different days. Age of control animals wt C99APP + wt PS-1 at median survival was 14 days, while that of V50F M51F C99APP + wt PS-1 was significantly shorter (10 days).

c. **Loss of synaptic puncta in V50F/M51F C99APP + wt PS-1 animals.** The average number of synaptic puncta per 100 μm in 'n' transgenic worms for each day is shown in the scatter plots for dorsal and ventral cords. The scatter plot displays all individual data points. Superimposed on the data are the mean values represented by the horizontal lines, with vertical bars indicating the standard deviation (SD). The 'n' for each day for a given mutant can be found in panel d. The number of synaptic puncta in dorsal nerve cord of V50F/M51F C99APP + wt PS-1 was significantly lower on day 1 (s= 18) compared to wt C99APP +wt PS-1 (s=21). Similar observations were seen until day 7 when there was no significant difference in s values between control and V50F M51F C99APP + wt PS-1. In the ventral nerve cord, on day 2 s=19 in V50F/M51F C99APP + wt PS-1 was significantly lower compared to s=21 in wt C99APP + wt PS-1. In the dorsal nerve cord, I45F C99APP + wt PS-1 and V44F/I45F C99APP + wt PS-1 animals had significantly lower s values compared to wt C99APP + wt PS-1 animals later, on day 3 and day 2 respectively. On day 7, there was no significant difference in s values between wt C99APP + wt PS-1 and V50F/M51F C99APP + wt PS-1 mutant in either nerve cord. ($p>0.05$ ns, $p\leq 0.05$ *, $p\leq 0.01$ **, $p\leq 0.001$ ***, $p< 0.0001$ ****). Note that in order to simplify visualization, data is plotted and statistics noted to indicate the earliest days on which significant differences occurred.

d. **Loss of synaptic puncta in V50F/M51F C99APP + wt PS-1 animals.** 100 μm sections of representative confocal images for wildtype (1st row) and transgenic animals are shown for days 1, 2, 3 and 7 for dorsal (left) and ventral (right). ‘s’ denotes the average of (number of synaptic puncta per 100 μm) from ‘n’ animals. Note the gaps in synaptic puncta in these images, increasing the distance between two consecutive puncta.

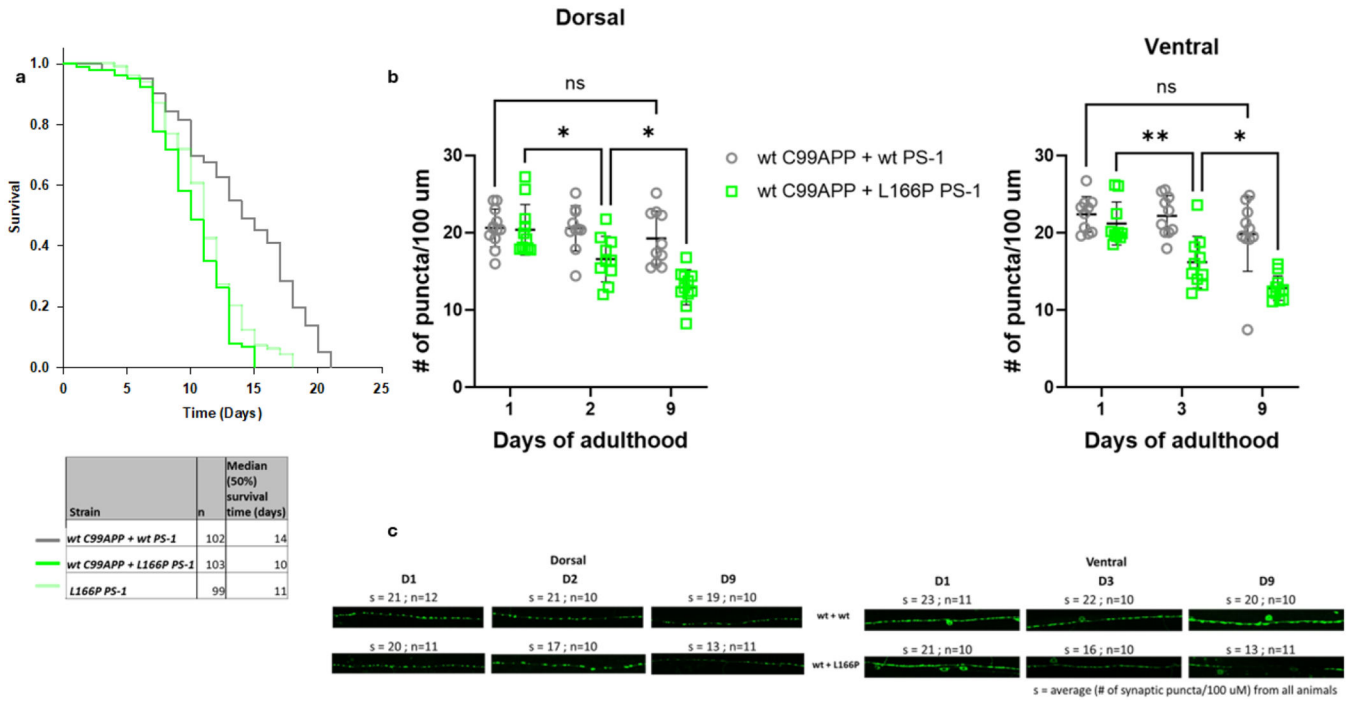

Strain	n	Median (50%) survival time (days)
wt C99APP + wt PS-1	102	14
wt C99APP + L166P PS-1	103	10
L166P PS-1	99	11

Figure 5. L166P PS-1 reduces lifespan independent of C99APP coexpression.

a. **Shorter lifespan of wt C99APP + L166P PS-1 animals.** Kaplan-Meier curves of 'n' animals show the fraction of animals alive on different days. Age of control animals (wt C99APP + wt PS-1) at median survival was 14 days, while that of wt C99APP + L166P PS-1 was significantly shorter (10 days). The median survival age of L166P PS-1 animals was 11 days.

b. **Age-dependent loss of synaptic puncta in wt C99APP + L166P PS-1 FAD animals.** The average number of synaptic puncta per 100 μm in 'n' transgenic worms for each day is shown in the scatter plots for dorsal and ventral cords. The scatter plot displays all individual data points. Superimposed on the data are the mean values represented by the horizontal lines, with vertical bars indicating the standard deviation (SD). The 'n' for each day for a given mutant can be found in panel c. In comparison to day 1, the number of synaptic puncta in wt C99APP + L166P PS-1 FAD animals reduced on day 2 significantly in the dorsal nerve cord and on day 3 in the ventral nerve cord. Age-dependent loss of synaptic puncta was seen in wt C99APP + L166P PS-1 FAD animals as the number dropped significantly on day 9 compared to day 2/3 in dorsal and ventral nerve cords. ($p>0.05$ ns, $p\leq 0.05$ *, $p\leq 0.01$ **, $p\leq 0.001$ ***, $p< 0.0001$ ****). Note that in order to simplify visualization, data is plotted and statistics noted to indicate the earliest days on which significant differences occurred.

c. **Age-dependent loss of synaptic puncta in wt C99APP + L166P PS-1 FAD animals.** 100 μm sections of representative confocal images for wildtype (1st row) and transgenic animals are shown for days 1, 2 and 9 for dorsal (left) and 1, 3 and 9 for ventral (right) nerve cords. 's' denotes the average of (number of synaptic puncta per 100 μm) from 'n' animals. In wt C99APP + L166P PS-1 dorsal nerve cord, on day 2, s value dropped significantly to 17, compared to s=20 on day 1. Similarly, the value of s dropped significantly to 16 on day

3 compared to 21 on day 1 in ventral nerve cord. Note the gaps in synaptic puncta in these images, increasing the distance between two consecutive puncta.

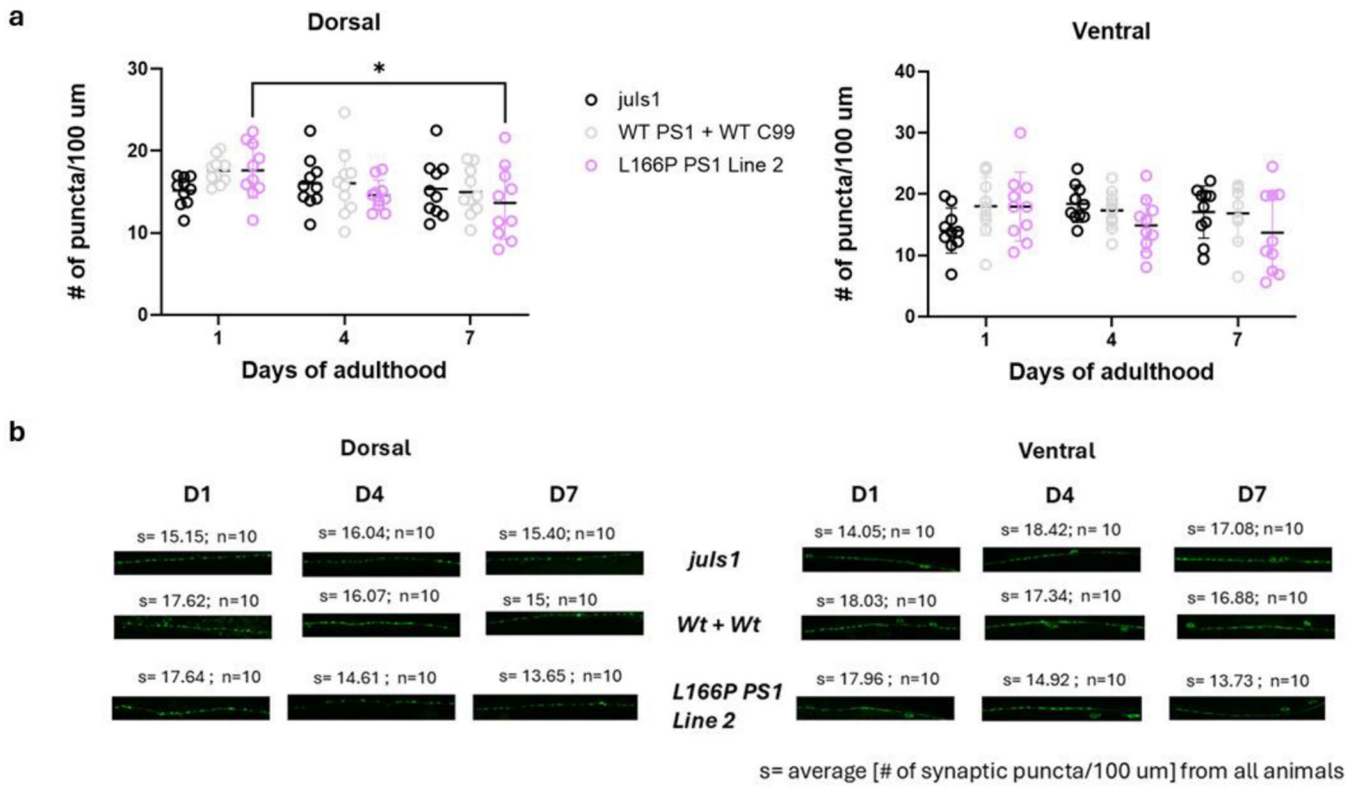

Figure 6. L166P without co-expression of WT C99 APP does not result in synaptic degeneration.

a. **Synaptic puncta quantification in L166P PS-1 monogenic animals.** The average number of synaptic puncta per 100 μm in 'n' transgenic worms for each day is shown in the scatter plots for dorsal and ventral nerve cords. The scatter plot displays all individual data points. Superimposed on the data are the mean values represented by the horizontal lines, with vertical bars indicating the standard deviation (SD). The 'n' for each day for a given mutant can be found in panel b. In comparison to wt C99APP + wt PS-1 control, the number of synaptic puncta in L166P monogenic animals is not significantly different on the days quantified (days 1, 4 & 7) in dorsal and ventral nerve cords. ($p>0.05$ ns, $p\leq 0.05$ *). There was some significant difference within the L166P strain itself: on day 7 of adulthood, the average number of synapses was significantly decreased as compared to day 1 within the strain ($p=0.0144$) for dorsal nerve cord. There were no significant differences for the ventral nerve cord.

b. **Synaptic puncta quantification of L166P PS-1 monogenic animals.** 100 μm sections of representative confocal images for controls (*juIs1* - 1st row & wildtype – 2nd row) and transgenic animals are shown for days 1, 4 and 7 for dorsal (left) and ventral (right). 's' denotes the average of (number of synaptic puncta per 100 μm) from 'n' animals.

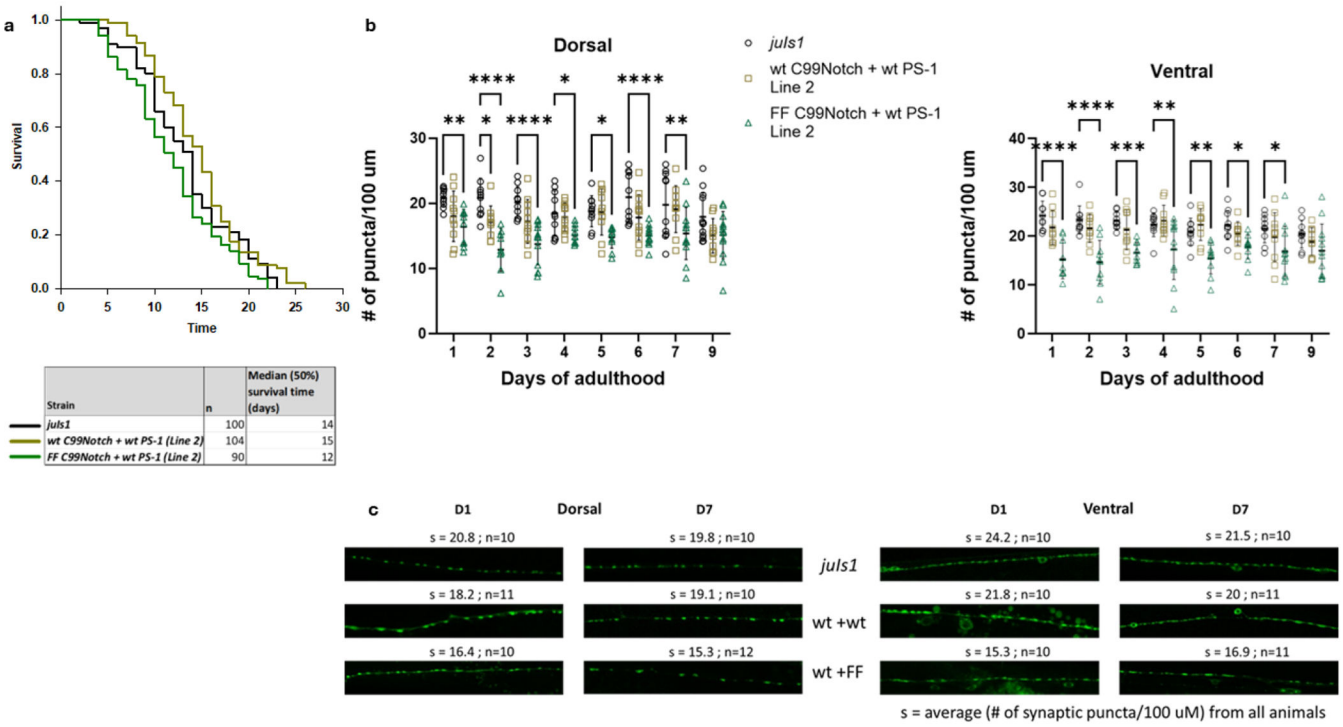

Figure 7. Expressing V50F/L51F (FF) C99Notch with wt PS-1 triggers synaptic loss and shorter lifespan.

a. **Lifespan of FF C99Notch + wt PS-1 animals.** Kaplan-Meier curves of 'n' animals show the fraction of animals alive on different days. Age of control animals – juIs1 and wt C99Notch + wt PS-1 at median survival was 15 days while that of FF C99Notch + wt PS-1 was 13 days. The survival curve was statistically different between wt C99Notch + wt PS-1 and FF C99Notch + wt PS-1 animals (comparison table in supplementary).

b. **Loss of synaptic puncta in FF C99Notch + wt PS-1 animals.** The average number of synaptic puncta per 100 μm in 'n' transgenic worms for each day is shown in the scatter plots for dorsal and ventral cords. The scatter plot displays all individual data points. Superimposed on the data are the mean values represented by the horizontal lines, with vertical bars indicating the standard deviation (SD). The 'n' for each day for a given mutant can be found in panel c. In comparison to *juIs1*, the number of synaptic puncta in FF C99Notch + wt PS-1 animals is significantly lower from day 1 until day 9 in dorsal nerve cord and day 7 in ventral nerve cord. ($p>0.05$ ns, $p\leq 0.05$ *, $p\leq 0.01$ **, $p\leq 0.001$ ***, $p< 0.0001$ ****).

c. **Loss of synaptic puncta in FF C99Notch + wt PS-1 FAD animals.** 100 μm sections of representative confocal images for wildtype (1st row) and transgenic animals are shown for days 1and 7 for dorsal (left) and ventral (right). 's' denotes the average of (number of synaptic puncta per 100 μm) from 'n' animals. In FF C99Notch + wt PS-1 dorsal nerve cord, on day 1, s value is significantly lower (s=16.7), compared to s=20.8 in *juIs1*. Similarly, the value of s is significantly lower in mutant C99Notch (s=11.8) on day 7 compared to *juIs1*(s=19.8) in dorsal nerve. Similar representative images can be seen for ventral nerve cord. Note the gaps in synaptic puncta in these images, increasing the distance between two consecutive puncta.

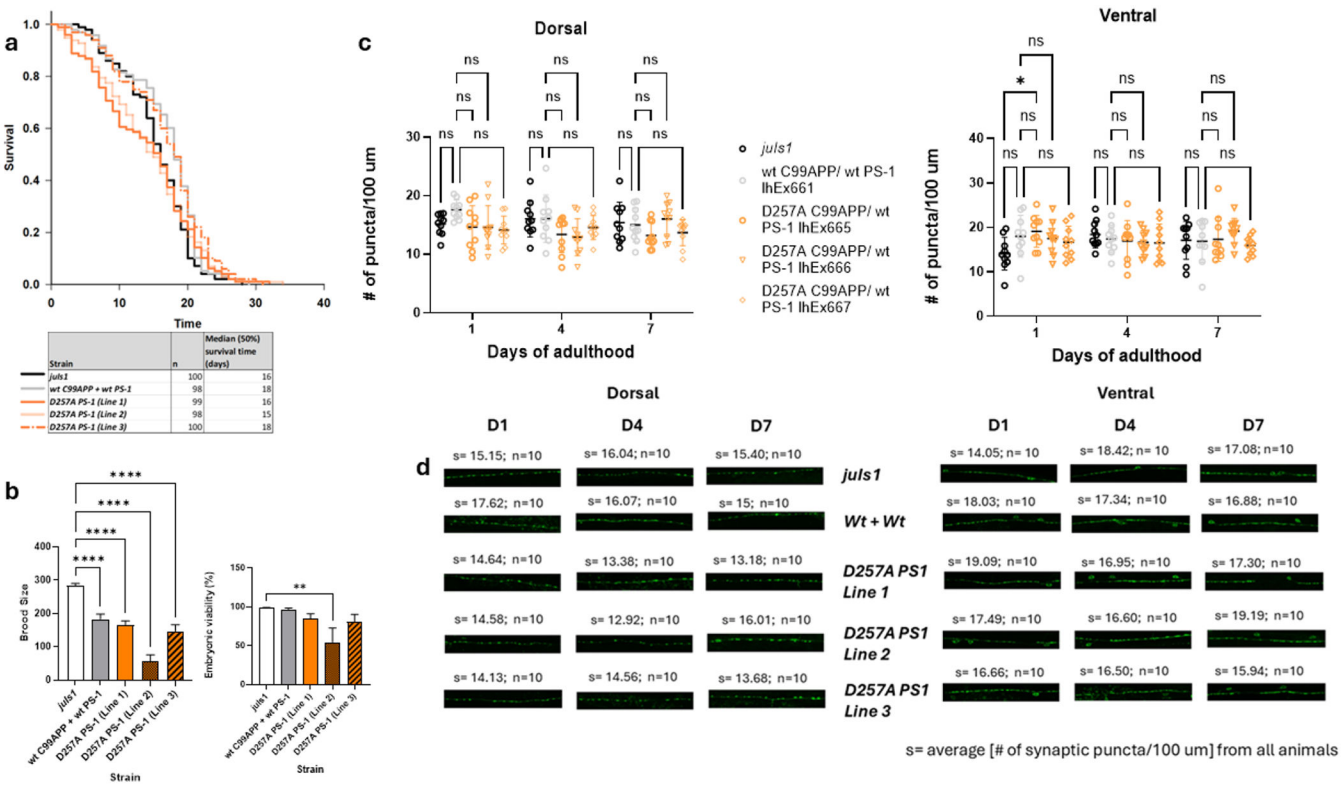

Figure 8. Catalytic aspartate mutation that eliminates proteolytic activity does not lead to a neurodegenerative phenotype.

a. **Lifespan of D257A PS-1 animals.** Kaplan-Meier curves of 'n' animals show the fraction of animals alive on different days. Age of control animals – *juIs1* and wt C99APP + wt PS-1 (Line 3) at median survival was 16 and 18 days, respectively. The survival curve of D257A PS-1 Line 3 is not statistically different when compared to wt C99APP + wt PS-1 control but is statistically different when compared to survival curve of *juIs1* animals (Table S7).

b. **Brood size and embryonic viability of D257A PS-1 mutant animals.** Final "n" values for animals: juIs1 (10), WT PS1 + WT APP C99 (10), D257A 1 (9), D257A 2 (6), D257A 3 (10). Animals that died before the 5 days of scoring were excluded from final analysis.

c. **Synaptic puncta quantification in D257A PS-1 animals.** The average number of synaptic puncta per 100 μm in 'n' transgenic worms for each day is shown in the scatter plots for dorsal and ventral cords. The scatter plot displays all individual data points. Superimposed on the data are the mean values represented by the horizontal lines, with vertical bars indicating the standard deviation (SD). The 'n' for each day for a given mutant can be found in panel d. In comparison to wt C99APP + wt PS-1 control, the number of synaptic puncta in D257A PS-1 animals is not significantly different on the days quantified (days 1, 4 & 7) in dorsal and ventral nerve cords. ($p>0.05$ ns, $p\leq 0.05$ *).

d. **Synaptic puncta quantification in D257A PS-1 animals.** 100 μm sections of representative confocal images for controls (*juIs1* - 1st row & wildtype – 2nd row) and transgenic animals are shown for days 1, 4 and 7 for dorsal (left) and ventral (right). 's' denotes the average of (number of synaptic puncta per 100 μm) from 'n' animals.